UNIVERSITÀ DEGLI STUDI DELL'AQUILA

DIPARTIMENTO DI SCIENZE FISICHE E CHIMICHE

Dottorato di Ricerca in Scienze Fisiche e Chimiche

XXXV ciclo

Material screening by Inductively Coupled Plasma Mass Spectrometry for characterization of background in low radioactivity experiments

SSD CHIM/03

Dottorando

Francesco Ferella

_____

Coordinatore del corso

Prof. Massimiliano Aschi

_____

Tutor

Prof. Marcello Crucianelli

_____

Co-Tutor

Ing. Stefano Nisi

_____

a.a. 2021/2022

Al nostro progresso

Contents

Abstract

Search for very rare astroparticle physics events, such as Neutrinoless Double Beta Decay or direct Dark Matter interactions demands for extremely low background environments and materials for the experiment construction. The former requirement is fulfilled by underground laboratories, such as the Laboratori Nazionali del Gran Sasso of INFN, where the overburden rock reduces the cosmic ray flux by six orders of magnitude with respect to the sea level. The latter requirement, i.e., the material selection and cleaning for low-background experiment, increasingly challenges the international scientific community to develop new purification techniques and push the sensitivity to the edge of instrumental limits. Indeed, given the variety of materials used for the construction of experiments (i.e., metals, plastics, electronics compounds, loaded liquids, pressurised gases) and the very low levels of radiocontamination required, versatile and cutting-edge purification and characterisation techniques are needed.

Inductively Coupled Plasma Mass Spectrometry (ICP-MS) is one of the most suitable technique for material screening because of its versatility and additional features such as high sensitivity (ppt level), short analysis time (days), small mass of samples (mg), possibility to acquire many elements simultaneously, and development of efficient analysis methods. Furthermore, several processes and chemical treatments are involved in the production of the raw materials, thus the effect of each step on the final product must be known in detail in order to be able to optimize the production protocol from the radiopurity point of view. ICP-MS is the only screening technique capable of investigating contaminations in all stages of production, for example separating bulk contaminations from surface ones by means of progressive chemical attacks.

In order to reach excellent results with ICP-MS, the workspace is crucial, because environmental contaminations must be avoided. For this reason, clean-rooms are ideal environment to perform both sample's treatment and characterization through ICP-MS.

My thesis work was developed at the Chemistry and Chemical Plants Service of the Gran Sasso National Laboratories. I was involved in the development of innovative techniques for the cleaning and characterization of materials. Especially of the X and Y experiments.

In the framework of the LEGEND experiment, highly enriched germanium crystals have been purified exploiting a chemical plant designed for this specific purpose. A sequence of chemical reactions was tuned to convert metal germanium crystals into high pure GeO2. The purification process was continuously monitored online by Inductively Coupled Plasma Mass Spectrometry (ICP-MS), in order to verify the purification efficiency and the conversion rate from starting material to final products.

Moreover, another material widely used to build inner structures and external shields of astroparticle physics experiments is copper, which is one of the most radiopure metal, easy to machine and suitable also for cryogenic applications. Given the extremely low contaminations in thorium and uranium (10−12 – 10−15 g/g) in copper, different approaches must be developed in order to reach low detection limits at a level of 0.4 - 1 × 10−12 g/g). In this thesis, pre-concentration methods based on matrix extractions were developed to maximize quantification of Th and U in several samples of copper. On the other hand, also different materials (plastic, metals, organic) have been characterized through ICP-MS analysis, developing different treatments to solubilize them.

1 Scientific Cases

The rare event physics is currently focused on two hot topics in Astroparticle Physics, i.e., Neutrinoless Double Beta Decay and Dark Matter interactions detection. While the former is a very rare nuclear process whose discovery would clarify the fundamental nature of the neutrinos, the latter would explain the composition and properties of about 90% of the mass in the Universe. Finally, the same underground laboratories developed for Astroparticle experiments are also suitable for biological studies dedicated to understanding the effect of radioactivity on cells. In this chapter, the aforementioned scientific cases are briefly introduced.

1.1 Neutrinoless Double Beta Decay

Neutrinoless double beta decay (0υββ) is related to lepton number violation (LNV), LNV is a factor to be considered for some reasons, lepton number is only an accidentally conserved global symmetry in Standard Model (SM) and its conservation in extended theories seems very unlikely. Furthermore, in grand unified theories lepton and baryon number are often connected, almost all mechanism that generate and suppress neutrino masses result in Majorana neutrinos and thus eventually induce 0υββ decay. All theories beyond Standard Model (SM) violate lepton number by one or two units lead to neutrinoless double beta decay, global symmetries are not expected to be conserved in quantum gravity theories[33].

Search of 0υββ decay is considered as most promising way to prove Majorana nature of neutrinos as well as to give an indication a mass hierarchy and on absolute mass scale; discovery of 0υββ decay would open way for theories predicting observed matter anti-matter symmetry of Universe being a consequence of lepton number violation through leptogenesis [34].

Neutrino oscillations conserve lepton number and cannot distinguish between Majorana and Dirac particles; to test this symmetry and to establish nature of neutrinos, it's

necessary to search processes able to break lepton number. Neutrinoless double beta decay turns out to be most sensitive. Regarding decay process, transition of nucleus with mass and atomic numbers A and Z occurs to a nucleus with A and Z + 2 with emission of electrons. Violation of electron lepton number is related to two units:

$$(A, Z) \rightarrow (A, Z + 2) + 2e^{-}$$

Otherwise, in double beta decay are also emitted two neutrinos together with two electrons:

$$(A, Z) \rightarrow (A, Z + 2) + 2e^{-} + 2\bar{\nu}_e + Q_{\beta\beta}$$

where $Q_{\beta\beta}$ is energy released.

While double beta decay doesn't violate lepton number, neutrinoless double beta decay violets lepton numbers by two units and it's not allowed by SM; from this evidence, it could be said neutrino is a Majorana particle, unlike all other fermions in SM.

Considering natural elements reported in Periodic Table of Elements, some elements have isotopes that can decay through neutrinoless double beta decay[35], Table 1.

Table 1 Isotopes mostly used in 0υββ decay experiments, with relevant parameters and features

Double-beta candidate	Q-value (MeV)	Phase space G_{01} (y^{-1})	Isotopic abundance (%)	Enrichable by centrifugation	Indicative cost normalized to Ge
^{48}Ca	4.27226 (404)	6.05×10^{-14}	0.187	No	—
^{76}Ge	2.03904 (16)	5.77×10^{-15}	7.8	Yes	1
^{82}Se	2.99512 (201)	2.48×10^{-14}	9.2	Yes	1
^{96}Zr	3.35037 (289)	5.02×10^{-14}	2.8	No	—
^{100}Mo	3.03440 (17)	3.89×10^{-14}	9.6	Yes	1
^{116}Cd	2.81350 (13)	4.08×10^{-14}	7.5	Yes	3
^{130}Te	2.52697 (23)	3.47×10^{-14}	33.8	Yes	0.2
^{136}Xe	2.45783 (37)	3.56×10^{-14}	8.9	Yes	0.1
^{150}Nd	3.37138 (20)	1.54×10^{-13}	5.6	No	—

1.1.1 History

Regarding knowledge of neutrinos, in 1930 Wolfang Pauli postulated a particle with spin ½ to explain continuous energy spectrum of electrons in B decay [36]; in 1933 Enrico Fermi developed the first theory about description of weak decays and weak interactions [37]; in 1937 Ettore Majorana introduced a new quantization for fermionic field [38].

There was a significant leap forward in 1953, when concept of total lepton number was introduced by Konopinski and Mahmoud for explanation of missing observation of some dacays [39]; subsequently, Pontecorvo suggested use of separate lepton numbers for electrons and muons. In 1957 Goldhaber measured helicity of neutrino [40]; finally in 1961 Glashow, Salam and Weinberg included neutrinos in SM as part of electroweak theory [41]. Nowadays, several different experiments exploiting various technologies and searching for transition in different isotopes exists as ^{76}Ge, ^{82}Se, ^{100}Mo, ^{130}Te [42,43].

1.1.2 Decay of ^{76}Ge isotope

In 0υββ decay search, germanium detectors are widely used due to their excellent energy resolution, compared to other competitive techniques; HPGe detectors are used in these works, they are made of high purity germanium crystals, more important peculiarity is high sensitivity to gamma rays. Using these detectors, high detection efficiency is achieved because Ge is detector and source of double-beta decay at same time. Nevertheless, some disadvantages arise when using germanium, energy of double-beta decay is low related to other isotopes as ^{208}Tl.

Different methods can observe 0υββ as direct, geochemical, radiochemical techniques, regards to geochemical methods [44], abundance of product nucleus is determined from minerals of known age containing precursor nucleus; differently, in radiochemical methods, abundance of product nucleus is measured in a suitable environment after many years from precursor nucleus. Anyway, in both methods it's not possible to distinguish double beta-decay and neutrinoless double beta-decay; instead in

direct experiments, from measurements of sum energy of two emitted electrons, double beta-decay is instantly detected by instrumentation.

First proposal of detection neutrinoless double beta decay was performed by Milano group in 1967 using $Ge^{8}Li$ detector [45–47]. In 1970's and 1980's several groups started their research focused on neutrinoless double beta-decay of ^{76}Ge with HPGe detectors with some tricks to reduce background [48–56].

In 1990's Heidelberg-Moscow and International Germanium Experiment collaborations [57–63] start their research using HPGe detectors with ^{76}Ge enriched crystals. Subsequently, GERDA and MAJORANA experiments continued this research based on ^{76}Ge until last years, reaching a sensitivity larger than 10^{26} yr.

Many steps forward have been made considering Ge detectors, several upgrades have been made to maximize performance and to be able to increase sensitivity of experiments. A low background obtained also thanks an efficient material screening is a determining factor in this type of research.

In the next years, LEGEND experiment will try to achieve sensitivity up to 10^{28} yr, progress and discoveries obtained in GERDA and MAJORANA experiments will be applied in setup of experiment.

1.1.3 0υββ experiments

In last years, neutrinoless double beta decay was largely studied by many experiments in all over the world; LNGS host for a long time several experiments searching neutrinoless double beta decay using different experimental approaches and apparatus. Especially for GERDA and LEGEND experiment, ICP-MS contribute was fundamental in order to make an accurate selection of various materials and crystals used in setup activities.

1.1.3.1 GERDA

GERDA (GERmanium Detector Array) experiment was installed in hall A at Gran Sasso National Laboratories, from 2011 to 2019 in different phases. Core of GERDA experiment was made of HPGe detectors isotopically enriched of ^{76}Ge up to 87% [64,65]; these detectors were directly immersed into liquid Ar, which acts both as a shield against external radioactivity and as a cooling medium.

Phase I GERDA (2011-2013) consisted of collecting and exposure of 23.5 kg*yr, 8 enriched semi-coaxial Ge detectors for a total mass of 15.6 kg were employed together with three non-enriched semi-coaxial detectors. An upgrade was carried out from 2013 to 2015 to improve sensitivity of 0υββ of ^{76}Ge beyond 10^{26} yr with an exposure of 100 kg*yr [66].

Phase II GERDA was meant to reach a background of order of 10^{-3} cts/(keV*kg*yr); detectors array used in this phase included 40 diodes in total, composed of 7 Phase I semi-coaxial detectors, 30 newly produced BEGes and 3 non-enriched semi-coaxial detectors. Data taking started at the end of 2015 and in 2018 achieving an exposure of 58.9 kg*yr, subsequently an upgrade was carried out with installation of five additional inverted coaxial detectors with total mass of 9.6 kg; data taking was resumed and lasted at the end of 2019 for a final total exposure of 103.7 kg*yr [67].

Experimental apparatus consisted of stainless-steel tank volume 590 m^3 filled with ultra-pure water as active veto, 66 photomultipliers tubes were also installed inside the tank; furthermore, scintillator panels were placed on the top of clean room to increase muon veto system [68]. Water tank contained a stainless-steel cryostat filled with LAr, internal walls of cryostat were covered with pure copper layer to shield gamma radioactivity originating from steel. Germanium detectors were arranged in seven strings surrounded by a cylindrical nylon vessel conceived to reduce collection of ^{42}K ions; electronic part was performed using 90 silicon photomultipliers and 16 photomultipliers. Readout of germanium detectors was performed using charge sensitive amplifiers located in LAr.

1.1.3.2 MAJORANA DEMONSTRATOR

MAJORANA Demonstrator is an experiment located at Stanford Underground Research Facility (SURF). This experiment searches for 0υββ decay of ^{76}Ge with HPGe [69], it implemented an array of 58 HPGe detectors for a total mass of 44.8 kg arranged in two different modules, each contained in a low background shield. Purpose of experiment was to determine whether a future 1 ton experiment could achieve a background goal of 1 cts*t*yr in 4 keV region of interest around 0υββ of ^{76}Ge, Q-value (energy released in decay) in 2039 keV.

Two low radioactive shields contained two modules of detector arrays, these shields were composed with electroformed copper and commercial copper alloy; outside copper shields, an additional high-purity lead shielding was enclosed in a region with LN_2 boil-off gas to reduce radon contamination. An active muon veto was located outside radon exclusion volume, and it was surrounded by normal polyethylene and polyethylene borate for neutron moderation. To achieve low background, MAJORANA Demonstrator used toal mass of 1196 kg of electroformed copper; materials used during construction of experiment were carefully screened and selected to be used for cabling, cryostat seals and all electrical and thermal insulations [70].

1.1.3.3 LEGEND

LEGEND (Large Enriched Germanium Detector for Neutrinoless double beta Decay) is a collaboration with purpose of build an experiment based on neutrinoless double beta decay of ^{76}Ge with a sensitivity of half-life beyond 10^{28} yr, to fully span inverted neutrino mass ordering region. Best experimental approaches and best characteristics developed and obtain in GERDA and MAJORANA will be used for setup of LEGEND, also collaboration is formed by mergers of two groups.

Regarding components level, LEGEND will exploit best results obtained during operation of GERDA and MAJORANA, specifically use of water Cherenkov veto and depletion of bare germanium detectors in an instrumented LAr volume; for electronic part, system

already tested in MAJORANA will be used to reduce background noise. However, a long and detailed material screening campaign is ongoing to find best materials with lowest level of contamination.

LEGEND consist of two phases: LEGEND 200 will use 200 kg of ^{76}Ge reusing GERDA infrastructure at LNGS, background that's expected is a factor 3 compared to observed value in GERDA (from 1.5 cts/(FWHM*ton*yr) to 0.5 cts/(FWHM*ton*yr)) and exposure of 1 ton*yr, LEGEND will be able to reach a sensitivity beyond 10^{27} yr. LEGEND 1000 will have an increase in mass of ^{76}Ge up to 1000 kg, background would be reduced to 0.025 cts/(FWHM*ton*yr) and exposure of 10 t*yr, sensitivity will able to reach 10^{28} yr. Location of LEGEND 1000 is still a discussion's topic inside collaboration.

Regarding infrastructure placed in hall A at LNGS, cryostat used in GERDA is able to host up to 200 kg of detectors divided into 19 strings; LEGEND-200 will deploy 20 kg of BEGes and 9.4 kg of ICPC detectors form GERDA and 28 kg of PPC detectors from MAJORANA; nearly 140 kg of newly produced ICPC detectors will be added. ICPC can be manufactured with a larger mass (~2 kg) with respect to BEGes (~0.8 kg) and PPCs (~0.85 kg). Reduced surface-to-volume ratio with respect to smaller detectors, makes ICPCs less susceptible to surface effects.

During 2018 upgrade, five ^{76}Ge enriched ICPC detectors were deployed in GERDA cryostat and operated in LAr for first time until end of data taking in 2019. After being tested and characterized, they showed energy resolution and background rejection capability comparable with BEGes while having a larger mass by a factor 3 [71,72].

1.1.3.4 CUORE

CUORE (Cryogenic Underground Observatory for Rare Events) is an experiment search for neutrinoless double beta decay of ^{130}Te. It's result of a long-standing activity focused on optimization of single particle thermal detectors (low temperature calorimeters) based on $^{130}TeO_2$ crystals absorbers. $^{130}TeO_2$-based bolometers have long been used in $0\upsilon\beta\beta$ decay searches, they have a very low heat capacity since they're dielectric and diamagnetic

kept at 10 mK and exhibit extremely good energy resolution, low intrinsic background and stability for several years. Furthermore, natural isotopic abundance of 0υββ decay of ^{130}Te (34.17%) [73] avoids needs for expensive isotopic enrichment at this stage.

Detection systems are composed by a close-packed array of $^{130}TeO_2$ thermal detectors at T ~ 10 mK, they're arranged in a cylindrical matrix of 19 vertical towers. Copper used to support crystals is a special alloy called NOSV with low concentration of radioactivity species, produced by AURUBIS company; nowadays, other experiments are also using this alloy in various constructions.

CUORE detector array is operated in vacuum inside a custom-made cryogenic apparatus that complies with very stringent requirements regarding lowest T, mechanical vibration levels, stability and radiopurity of used materials. As shielding, modern lead with NOSV copper and Roman lead are used inside cryostat. Background level reached in CUORE experiment turn out to be $1.49*10^{-2}$ cts*keV^{-1}*kg^{-1}*yr^{-1} [74].

1.1.3.5 CUPID

CUPID (CUORE Upgrade with Particle Identification) aims to increase source mass and reduce background obtained in CUORE, to search for neutrinoless double beta decay of ^{100}Mo. Sensitivity to achieve is 10-15 meV to effective neutrino mass, it's necessary a detector with an active isotope mass of order ton and background level ~ 10^{-1} cts/(ton*yr) in region 15 – 50 meV. Excellent energy resolution of bolometric technology, a scalability of bolometric detectors, a reproducibility of technical performance on technology, compatibility with CUORE infrastructure already existing at LNGS [75].

1.2 Dark Matter

In 1867, Isaac Newton published the treatise "Philosophiae Naturalis Principia Mathematica", containing Newtonian laws of motion and theory of gravity[76]; he provided tools to detect unseen or invisible objects through their gravitational influence on other

bodies. An astonishing application is from 1846, when French and English astronomers Urbain Le Verrier and John Couch Adams proposed existence of an unseen planet, in order to explain anomalous orbit of Uranus [77]. Indeed, their German colleague John Galle could identify planet of Neptune very night after receiving a letter with instructions of where to look [78].

In early 20th century, many astronomers speculated and attempted to measure amount of dark matter in our own galaxy; in 1930, Swedish professor Knut Lundmark measured rotational velocities of five galaxies, and found mass that was necessary to keep galaxies stable were many times larger than that value of visible matter [79]. In 1970, Vera Rubin made more detailed measurements of rotational velocities in spiral galaxies, and how rotational velocity varies as a function of galactocentric radius [80].

Dynamical measurements such as these are still one of most intuitive and compelling pieces of evidence for non-collisional dark matter. In same way, dynamical mass measurements of spheroidal dwarf galaxies or spiral galaxies using satellite probes such as globular cluster traces gravitational potential and mass distribution. Today we have strong evidence that most of matter in Universe is dark, also there's evidence for dark matter in a vast range of distance scales, ranging from sub-galactic to cosmological scale [81].

1.2.1 Candidates

All particles that we know to exist are described by Standard Model [82], this model is a hugely successful theory, although it has some shortcomings: it describes three of known forces of nature, but not gravity.

In general, particle dark matter must be weakly interacting and invisible and stable enough not to decay over current age of Universe. One class of particle considered in dark matter studies are called Weakly Interacting Massive Particle (WIMP), it's somewhat of an umbrella term; they refer to a particle that interacts with Standard Model particles via weak nuclear force, typically thermally produced by freeze-out in early Universe and with a mass of around 100 GeV [83].

Axion is another well studied dark matter particle candidate, it was introduced in order to solve another fine-tuning problem of Standard Model; axion is a boson and would be very light, of MeV mass or lighter. Other possible dark matter candidates are heavier sterile neutrinos that don't interact via weak force but through neutrino oscillations.

1.2.2 Detection

There's a large global effort to detect particle dark matter non-gravitationally, particle dark matter is sought in experiments with collider, and also in direct and indirect detection experiments; in fig. 4 there are represented these three strategies, different types of interactions and set complementary limits to dark matter particle models.

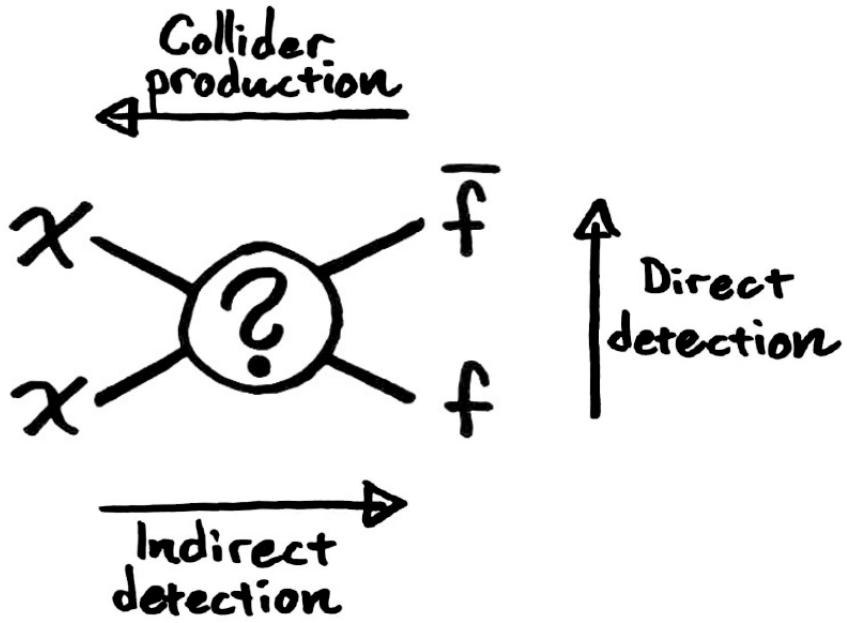

Fig. 4 Three different strategies for detecting particle dark matter

Particle dark matter can be produced in a particle collider, given that mass of dark matter particle is within reach of collider's energy; dark matter is searched for in terms of missing energy and momentum, a sign that something very weakly interacting has been produced and escaped undetected [84–86].

In direct detection, a dark matter particle can scatter against detector material and deposited energy can be measured. In noble gas detectors, a dark matter particle could cause excitation or ionization in detector medium. Furthermore, there are also methods of indirect detection, whereby dark matter particle decay or annihilation could be inferred from detection of Standard Model particles. For example, high energy photons coming from dark matter annihilation could make a convincing signal, as energy and directional origin can be well resolved. In addition, other products of dark matter annihilation could be cosmic rays, meaning high energy particles as protons, electrons, or neutrinos. Detection of anti-matter/cosmic rays would be especially telling because background of anti-matter particles from other sources is very low.

1.2.3 Experimental approaches

Several designed detectors with various target materials are begin used to search for WIMP dark matter [87].

Large target masses can be realized by using arrays of high-purity scintillator crystals, mainly NaI(Tl) and CsI(Tl), high mass number of Iodine and Cesium lead to a high sensitivity to spin-independent interactions; shortcomings of these detectors are a comparatively high intrinsic background level and absence of feudalization and electronic recoil rejection. Experiments thus concentrate on exploiting annual modulation signature to identify dark matter signal.

Germanium and silicon semiconductor ionization detectors are used to search for dark matter induced charge signals. Just a very small amount of energy is needed to create an electron-hole pair which leads to an excellent energy resolution; furthermore, signals exhibit a rather slow time constant and capacitance of diodes, leading to high electronic noise, doesn't allow building detectors beyond few-kg scale.

Crystalline cryogenic detectors (bolometers) measure heat of athermal phonon (depending on temperature sensor) signals by measuring tiny particle interaction-induced measuring energy released from particle converting into phonons. Dielectric crystals with

good phonon-transport property are particularly well-suited for cryogenic operation. Several methods to measure ΔT are available, frequently used are transition energy sensor (TES) for athermal phonons and neutron transmutation doped (NTD) germanium thermistors for heat thermal phonons. Cryogenic detectors feature a precise energy measurement with almost no quenching in heat channel, excellent energy resolution and background rejection down to energies.

Noble gases argon and xenon are excellent scintillators and can be ionized easily. In liquid they are used to build massive, dense and compact dark matter targets which already exceeded ton-scale. Interactions produce heat and excite (X*) and ionize (X^+) atoms. X* form excimer states X_2* with neutral atoms X. These decay under emissions of ultraviolet light at a wavelength of 128 nm and 178 nm for argon and xenon respectively. Photocathode materials with sensitivity to xenon scintillation light exist but wavelength shifters such as tetraphenyl-butadiene (TPB) must be used for argon, fig 5.

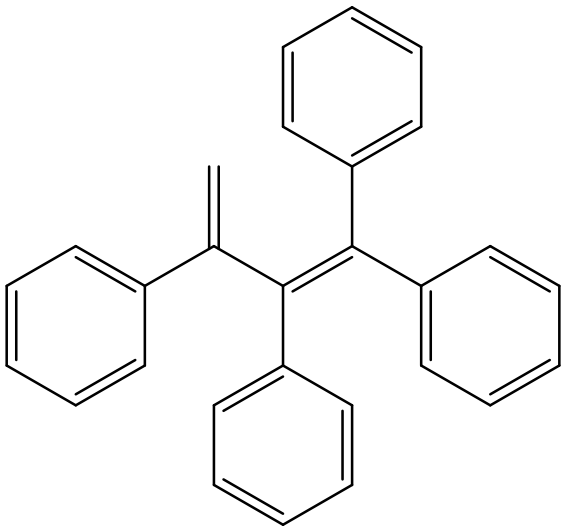

Fig. 5 tetraphenyl-butadiene (TPB)

Single-phase liquid nobel gas detectors measure only scintillation signal: to optimize light collection efficiency, a spherical target is surrounded by photomultipliers. Interaction position can be reconstructed via photon timing and signal distribution with few resolutions. Single-phase argon detectors additionally employ PSD for background reduction. Dual-phase

time projection chambers (TPC) measure primary scintillation signal as well as ionization electrons.

Superheated liquids are used as target material in bubble chambers, liquids are kept at T values just above their boiling point such that a local phase transition will create a bubble if energy above some threshold is deposited into a certain micro-volume. Superheated droplet detectors employ same detection principle, their bubbles are trapped in a water-based polymer matrix [88] which reduces dead time.

Directional detectors aim reconstructing direction of WIMP-induced nuclear recoil [89,90]. As track length depends on target density and longer tracks facilitate reconstruction of directionality, most directional detectors feature low-pressure gas targets with photographic or fine-granularity track readout in a TPC geometry.

1.2.4 Dark matter experiments

Regarding identification of dark matter, several experiments have been conducted and are still ongoing at various underground laboratories around the world; some experiments will be briefly described where there was a contribution with ICP-MS analysis.

1.2.4.1 XENON

XENON1T experiment operated underground at INFN – Gran Sasso National Laboratories from 2016 to 2018 [91], using a dual-phase LXe TPC with a 2.0 tons active target to search for rare processes. A particle interaction within detector produces both prompt scintillation and delayed electroluminescence signals. These light signals are detected by bottom of active volume and they are used to determine deposited energy and interaction position of an event. Latter allows for removing background events near edges of target volume through feudalization. Ability to determine scatter multiplicity enables further reduction of backgrounds, as signals are expected to have only single energy deposition.

XENONnT was designed as a fast upgrade of its predecessor [92] and shares many of systems and infrastructure. For instance, XENON1T systems for cooling, gas storage, purification and Kr-removal are all used for XENONnT. Core of experiment is a new dual-phase xenon time projection chamber (TPC), enclosed in a double-walled stainless-steel cryostat filled with LXe. A neutron veto was added, surrounding cryostat, to detect gammas produced from neutron capture of gadolinium. Moreover, an extensive material radioassay campaign [93] was conducted on it, a new high-flow radon removal system was developed to further reduce this background [94].

1.2.4.2 DARWIN

DARWIN will be an experiment using a multi-ton liquid xenon TPC, with primary goal to explore experimentally accessible parameter space for WIMPs, DARWIN will measure WIMP-inducted nuclear recoil spectra with high statistics and constrain mass and scattering cross section of dark matter particle[95]. Other physics goals are real-time detection of solar pp-neutrinos with high statistics, detection of coherent neutrino-nucleus interactions, searches for solar axions and galactic axion-like particles (ALPs) ad search for neutrinoless double beta decay. Facility will also be able to observe neutrinos of all flavors from supernova explosions[96], providing complementary information to large-scale water-Cherenkov or LAr detectors. Experiment will operate a large volume of LXe in a low background cryostat, surrounded by concentric shielding structures. Core of experiment is a dual-phase TPC containing active Xe mass, high density of LXe results in a short radiation length and allows for a compact detector geometry with efficient self-shielding. TPC will be housed in a double-walled cryostat made of stainless steel, titanium or copper, and all materials are to be selected for ultra-low intrinsic radioactivity.

1.2.4.3 COSINUS

COSINUS (Cryogenic Observatory for Signatures seen in Next-generation Underground Searches) experiment aims at detection of dark matter-induced recoils in

sodium iodide (NaI) crystals operated as a scintillating cryogenic calorimeter. Construction of experiment facility started in 2021 at INFN – Gran Sasso National Laboratories [97]. It consists of a cryostat housing with calorimeters made-up by crystals of NaI inside, they shielded from external radioactivity by a water tank acting also with an active veto against cosmic ray-induced events. Environmental radioactivity and intrinsic contamination of materials used for cryostat were checked by several screening campaigns performed by low radioactivity techniques in different times; an estimation of background level was reached at the end of preliminary study. Evaluation of number of events that could mimic or interfere with signal detection while optimizing geometry of experimental setup was also reached [98].

1.2.4.4 CRESST

CRESST (Cryogenic Rare Event Search with Superconducting Thermometers) aims to directly detect WIMPs via their elastic scattering on nuclei in a proper target material. Major challenges for such an experiment are low energies expected from WIMP interactions, low interaction rates and background from natural radioactivity or cosmic radiation. Cryogenic detectors were chosen to allow measurements of low energies with good resolution [99]. Most of background coming from ionizing radiation, which mainly interacts with electron target system. So, material for detector chosen by CRESST collaboration is $CaWO_4$, which is a good scintillator also al low temperatures and contains heavy element tungsten as a suitable target for WIMP interactions. Experimental setup consists of $^3He/^4He$ dilution refrigerator with separated large detector volume connected by a cold finger. Detector volume is surrounded by a heavy copper and lead shielding, including some lead inside cryostat, to block direct line of sight between active parts of refrigerator and detectors [100].

1.2.4.5 SABRE

SABRE (Sodium iodide with Active Background REjection) is a direct detection dark matter experiment based on arrays of radio-pure NaI(Tl) crystals. Experiment aims at achieving an ultra-low background rate and its primary goal is to confirm or refute results

from DAM/LIBRA experiment. This experiment is designed to measure dark matter annual modulation interaction rate with achievement of ultra-low background. Direct dark matter detectors are suitably well-shielded against external radiation and their background rate is driven by radioactive contaminants in detector material and in materials used for construction of experimental setup. Such radioactive contamination may come from long-lived, naturally occurring isotopes of from cosmogenic activation; careful selection or development of radio-pure materials and equipment is therefore mandatory, as well as a detailed knowledge of residual radioactivity. NaI(Tl) crystals adopted for SABRE, photosensors and all detector materials are designed to reach ultra-high radiopurity levels; a liquid scintillator veto allows for an active rejection of residual background [101].

1.3 Underground Biology

Originally Deep Underground Laboratories (DULs) were built to host astroparticle and nuclear physics experiments requiring a low background environment and largely reduced levels of cosmic ray particle interference. The unique underground environment has attracted the attention of a wider scientific community interested to conduct multidisciplinary experiments in ultra-low radiation environment, including radiobiology. In radiobiology contest, studies in DULs could lead to important fallouts in very low dose/dose rate radiobiology and in the optimization of exposure conditions to radiations.

Nowadays, experiments located in DULs are characterized by having procedures of radioprotection that are currently founded on assumption that risk is directly proportional to dose [102]; an ideal scenario for extremely low dose/dose rate investigations. Up to now, interesting results have been obtained in protozoan, bacteria, yeasts, mammalian cells of rodent and human origin [103] comparing biological responses of these biological models in underground low radiation environment respect to external reference environment.

At Gran Sasso National Laboratories, a facility for underground biology experiments was installed many years ago, called PULEX[104]. This facility was created for cell culture and *in vitro* experiments where the radon concentration was kept low as the reference

environment (external facility) by an air ventilation system in addition to two CO_2 incubators (one of this shielded by iron).

More recently a small animal housing was built nearby PULEX, called COSMIC SILENCE. The new facility is provided with temperature and light control systems and an improved air-ventilation system. This laboratory provides opportunity to investigate effects of reduced natural background radiation at level of whole organism. In radiobiology experiments, characterization of environments of which biological tests are carried out is extremely important: dosimetry measurements are carried out to monitoring level of radiation in experimental halls as well as radon concentration, pressure, temperature and relative humidity are continuously monitored.

1.3.1 Underground Radiobiology activity

Radiobiology is a multidisciplinary science that studies effects of ionizing radiation on biological tissues and their cellular and molecular components [105]. In particular, underground radiobiology is referred to biological studies conducted in DULs; its aim is to investigate effects of natural environmental ionizing radiation background on living organisms [106]. In 1995 at LNGS a first pioneering study was carried out by prof. Luigi Satta on yeasts and showed a higher frequency of mutation rate in cells grown in underground respect to reference environment [107]. In 2002 a study was conducted on mammalian cells, V79 Chinese hamster cells, and reported significative difference in term of biochemical responses in low background radiation cells [108]. Over the time, other experiments on biological systems were conducted in underground laboratories such as WIPP in New Mexico, SNOLAB in Canada [109] and DULB-4900 in Russia [110,111].

In all experiments, a different behaviour of biological models used was observed in underground respect to external reference environment suggesting an important role of natural environmental radiation on metabolism and efficiency of biological responses to stress of living organisms.

1.3.1.1 FLYINGLOW PROJECT

Flyinglow project, funded by Centro Fermi, was a research program to determine whether LNGS underground environment could affect different life parameters in the multicellular model, *Drosophila melanogaster.* Choice of *Drosophila* model in this investigation was made because fruit fly is a very powerful model in study of genes in diseases and a suitable model to evaluate the biological effects following exposure to radiation. The published results showed that reduction of environmental radiation affects developmental parameters of *Drosophila*, providing evidence for first time on influence of radiation background in a complex organism [112].

From the comparison between the biological parameters such as life span, locomotion activity and fertility in two different environments (underground versus above ground), it was revealed that average life span of flies in underground was longer than flies located above ground although the fertility, both in males and females, was significantly lower in the underground environment. Many important goals were achieved in this study: for first time a multicellular organism was used in these underground investigations, a biological response was observed also at whole organism level and *Drosophila* was proved to be a very good model for underground radiobiology experiments. Today, other DULs are using Drosophila as model system in their biology experiments [113,114].

1.3.1.2 RENOIR

RENOIR (Radiation Environment Triggers Biological Responses in Flies) experiment aimed to improve knowledge of environmental radiation spectrum in underground and above ground environment and to investigate specific role of gamma component on biological response of *Drosophila melanogaster* as *in vivo* model system. Several aspects were examined during installation and function of experiment with particular attention to total contribution of radiation, examining it in different characteristics.

Regards to cosmic rays, contribution of above ground reference radiation environment is ~ 41 nSv/h (specially muons), about neutrons is ~ 21 nSv/h, on terrestrial

gamma ray is ~ 22 nSv/h; differently, for underground low radiation environment contribution of cosmic rays and neutrons are strongly reduced respect to underground environment and considered negligible, while gamma dose rate is ~ 20 nSv/h [103]. In addition, ^{222}Rn contribute to environmental dose rate with its decay products, however inside the underground facilities an efficient ventilation system is running to maintain radon concentration comparable to external environment. Moreover, Monte Carlo simulations are used to have a complete overview on radioactive environments.

In order to obtain information about the influence of gamma component of radiation spectrum on biological response of Drosophila, special devices are used to modulate the gamma spectrum. To further reduce the gamma component, a thick lead hollow cylinder was modified and equipped with a properly designed ventilation system to prevent accumulation of radon and a control system for T and light in order to maintain Drosophila culture inside it. On the other hand, to increase gamma component, a customized Marinelli beaker was designed and built. Marinelli beaker was filled with tuff and pozzolana (natural gamma-emitters) and sealed to avoid radon exchange. Also for this case, simulations on Marinelli beaker geometry helped for design and also to characterization of total radioactive contribution.

A recent publication [115] showed that reduced radiation background of LNGS underground laboratory renders Drosophila cells more sensitive to an induced DNA damage compared to external reference laboratory fruit flies. DNA damage sensitivity of underground flies was rescued by increasing the underground gamma dose rate using the Marinelli device. This study provided direct evidence that damage response in a complex multicellular organism is dependent on the environmental dose rate radiation.

2 Backgrounds in Rare Event Search

As discussed in the previous chapter, the physics of rare events search for very rare decays ($T_{1/2} \sim 10^{27}$ yr) or particle interactions with very small cross sections (probability of interaction). Therefore, the expected signal in these experiments is lower than 10 events per year. Since the expected signal cannot be easily increased, it is necessary to reduce the background. In this chapter, the dominant sources of background in rare event physics are discussed.

2.1 Characteristics

Improving background reduction, through an accurate analysis of surrounding environment, material plays a very important role in rare fundamental physics phenomena like neutrinoless double-beta decay and dark matter interaction; very low levels of background radiation are required to observe a signal. An important factor is related to decay time ($T_{1/2}$), required time for half original population of radioactive atoms to halve. For such rare process ($T_{1/2} > 10^{20}$ yr), sensitivity of measurement depends critically on background level in interest area; natural radioactivity from surroundings setup materials and detector itself are source of alfa, beta, gamma, and neutrons (^{232}Th $T_{1/2} \sim 10^{9}$ yr, ^{235}U $T_{1/2} \sim 10^{8}$ yr, ^{238}U $T_{1/2} \sim 10^{9}$ yr, ^{40}K $T_{1/2} \sim 10^{9}$ yr, etc). Further, muon-induced interactions in materials surrounding detector give rise to additional background of gamma-rays and neutrons; while it's possible to eliminate these background sources, reduction of background becomes essential to improve sensitivity. Flux of muons in cosmic ray can be significantly reduced in an underground laboratory, due to natural shielding as rock mountain; background coming from internal sources can be minimized by careful selection of radiopure materials[1,2], instead background coming from external sources is reduced by suitable shielding [3]. In many astroparticle physics experiments, ultra-low background levels in the order of $< 10^{-3}$ cts/(keV*kg*yr) have been achieved using special materials and novel techniques [4,5]. Total contribution on background must be taken into consideration during data analysis. Generally, a background model employing Monte Carlo simulations

considering all contributions from actual step and environment in experimental site is used for physics analysis [6–9].

During installation of experiment, one of principal purpose is to achieve an environment with “zero background”, with total no contribution of radiation; materials are subjected to a punctual screening process to evaluate their purity, for this reason they’re carefully chosen by operators. Design of experiments aims for “zero background” such that observation of a few signal events would already have a high statistical significance, being experiments that search for rare events, an environment with as little contamination as possible is strictly necessary; direct achievement of “zero background” level is not possible, however use of selected materials and correct handling can considerably reduce contaminations. Among various background source are found: Electronic Recoil Background, α-Background, Nuclear Recoil Background, Radiogenic neutrons, Cosmogenic neutrons. Regarding Background Mitigation, different approaches can be applied to maximize sensitivity of experiments: Shielding, Material Selection, Target Purification, Active Rejection.

Shielding of underground laboratory is carried out mainly by overlying rock, considering thickness level and altitude of each laboratory; diversity of these characteristics makes each laboratory suitable for certain astroparticle physics experiments with certain levels of sensitivity. Classification of depth is expressed by “meters water equivalent” (m.w.e.), shown in fig. 1.

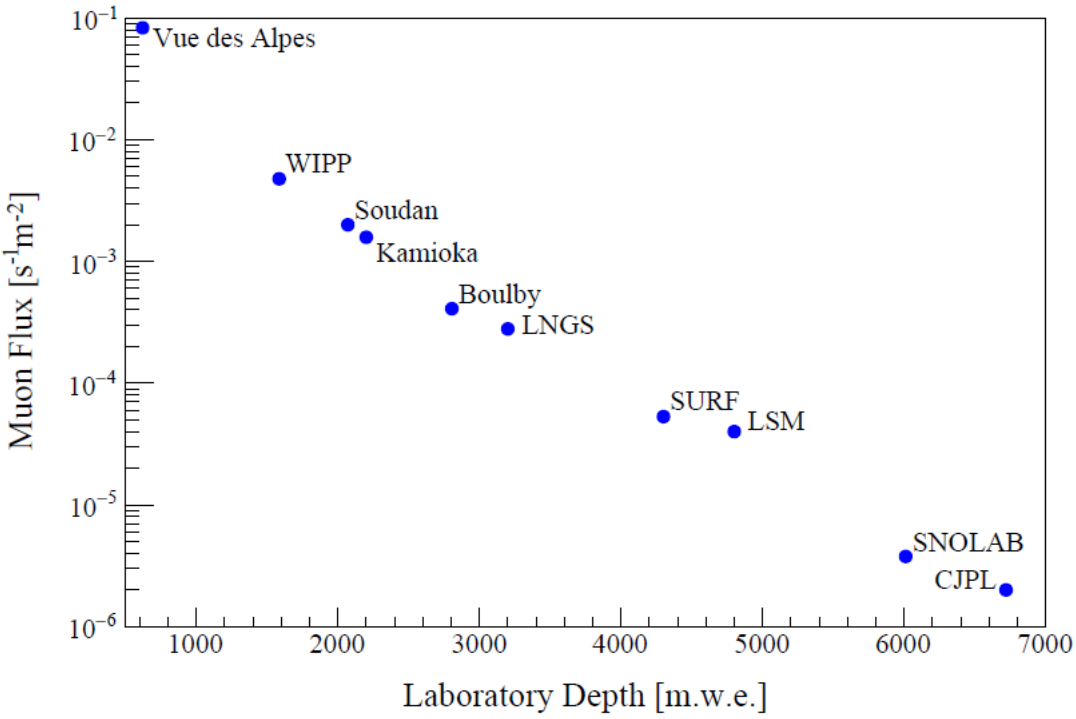

Fig. 1 Muon flux vs depth of various underground laboratories

To improve shielding, low intrinsic radioactive contamination materials are used for assembly of experimental apparatus; there're various material screening techniques, each specific to a certain type of analysis. Moreover, other characteristics vary according to adopted technique: sample preparation, analysis time, sensitivity, etc.

Experiments require high radiopure materials to observe rare event searches, so R&D is ongoing on this field of application; moreover, a possible way to follow is related to use of deep underground laboratories in order to remove atmospheric backgrounds. Research on high pure materials proceed with a particular emphasis on finding those with lower content of natural radioactive elements as ^{232}Th, ^{238}U, ^{40}K. Regards on accurate determination of radio impurities, precise knowledge of detection efficiency is necessary to plan choice of type of materials to be used. It has been observed in the literature[10–15] that efficiency computed from Monte Carlo simulations using detector geometry supplied by manufacturer is overestimated (by ≥ 10%) as comparted to experimental values.

2.2 Background induced by cosmic ray

In physics experiment with background, sensitivity mean average upper limit that would be obtained by an ensemble of identical replicates of such an experiment, each one with same mean expected background and no true signal [16].

$$S(b) \equiv E[U(n|b)] = \sum_{n=0}^{\infty} Po(n|b) \cup (n|b)$$

where:

S(b) = sensitivity

E = background energy

b = mean predicted background level

n = given observation

U(n|b) = function yielding upper limit by unified approach

Po(n|b) = likelihood of individual observations

Sources of background must be thoroughly understood before starting an analysis, in order to minimize interferences and noise; it's also possible to divide background sources into more components: cosmic rays and neutrons, environmental radioactivity, radio impurities in detector, shield material, Rn and its progenies. Detectors radiopurity is a most important factor to consider as some radioactive elements generate decay chains; underground laboratories are right medium to reduce background, rock shielding and conformation of upper environment can improve background.

In earth's atmosphere, a great presence is due to cosmic ray particles in a rate about 1000 $m^{-2}s^{-1}$; they have an interaction with atmospheric atoms generating variety of elementary particles: neutrons, electrons, neutrinos, protons, muons, pions. Total intensity of these secondaries particles reaches a maximum at an atmospheric depth of about 150 g/cm^2 and then falls off gradually, with nucleons experiencing sharpest decline.

Regards low background techniques, only muons and neutrons are relevant in underground environment, as Gran Sasso National Laboratories of INFN (National Institute for Nuclear Physics). Electrons, protons and photons are directly absorbed by lead shield or by overburden from building ceilings. Neutrons are attenuated with a mean length of ~ 200 g/cm [17], muons lose their energy in standard rock on a much longer scale, ~ 2 kg/cm^{-2} near sea level, by ionization, pair production, bremsstrahlung and nuclear interactions [18]. Furthermore, production of tertiary neutrons by muons in Pb shield is indicated as its flux of neutrons originating from natural fission; neutrons dominate in a massive Pb shield already below a few meters of water equivalent (m.w.e.).

Secondary cosmic ray particles can generate directly radioactive background via interactions with a detector, also indirectly through production of radionuclides. At sea level and even more during transport in air, activation by hadronic component can reach higher levels of specific radioactivity than residual contamination from primordial nuclides.

Study of cosmogenic production has its roots in meteoritic and lunar research, which has led to a profound understanding of production rates and it has simulated an extended compilation of cross sections needed to estimate these rates. Terrestrial in situ cosmogenic studies began two decades later, primarily because required sensitivity in three to four orders of magnitude higher.

In nuclear transformation of type $Z \rightarrow Z - 1$, there's strong contribution of stopped negative muons, it dominates nucleonic production at shallow depth. Production rate is related to stopping rate of negative muons, capture probability in target nuclei, emission probability for number of neutrons; fast muons produce energetic particle showers of protons, neutrons and π pions that can extend over several cubic meters of volume.

Background induced by cosmic rays (especially muons) is diminished by going underground; rock overburden reduces efficiently their intensity and their reaction products through interaction with matter (specially neutrons). Considering Gran Sasso National Laboratories, muon flux is suppressed by more than six orders of magnitude to less than 1 muon m^{-2}h^{-1} for energies up to 1 TeV [19], fig 2.

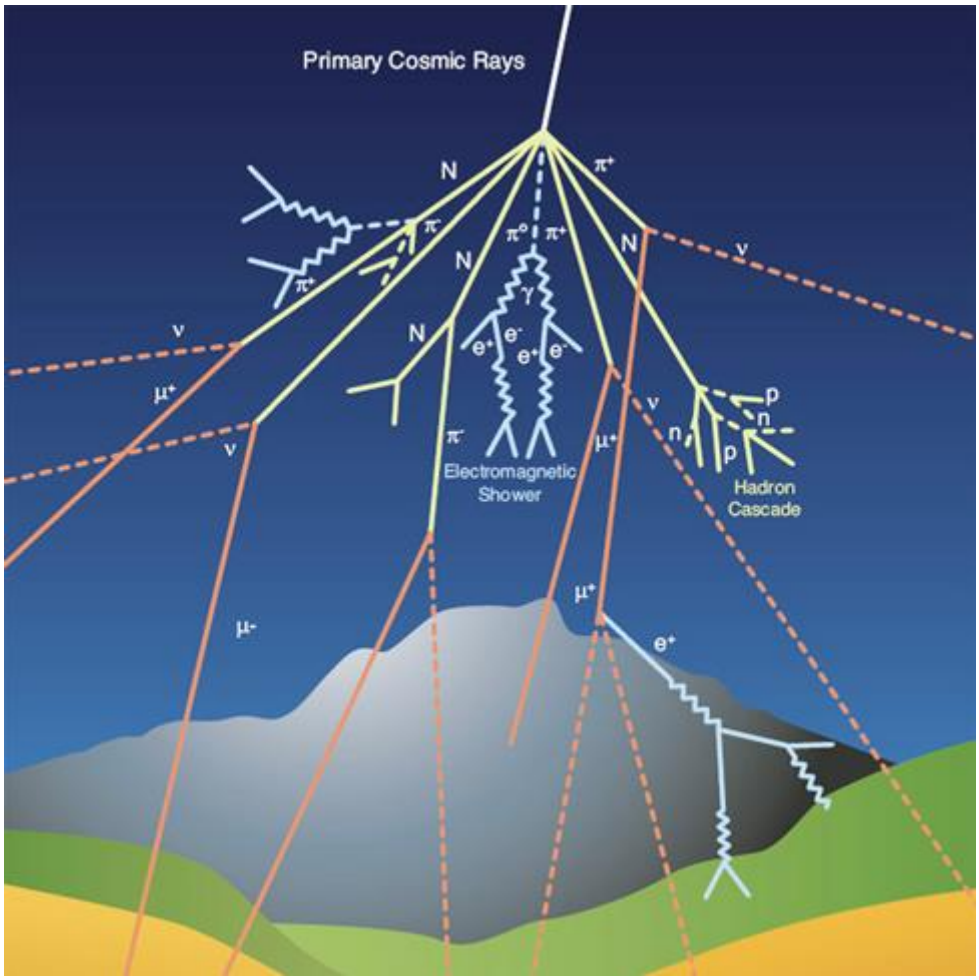

Fig. 2 Cosmic ray shield by rock mountain in Gran Sasso

Furthermore, inelastic scattering and radiative capture are main channels for direct neutron-induced background; in dark matter experiments searching for WIMPs [20,21], nuclear recoil can be faked by neutrons. Also in gamma-ray spectrometry, some systems are adopted to reduce neutron background, as use of neutron absorber in shield (borated polyethylene) depending on type of experiment and its overhead shielding.

An outside veto shield with a high registration probability for producing muons is effective in background suppression of neutron events, at least for Ge spectrometers at shallow depth with predominantly tertiary neutrons. Background contribution from neutron-induced radioisotopes with half-lives exceeding veto time is rather small, although not negligible for extremely sensitive experiments. If no moderator is present, tertiary neutrons may escape from shield before inducing a background event.

In WIMP search, background due to neutrons is much more severe, cryogenic detection technique, which is well suited for this task, is still in test phase and is therefore developed preferentially near home laboratory at shallow depth.

Otherwise, muons are decelerated almost exclusively by electromagnetic interaction with traversed matter; this deceleration results in high-energy electron/positron/photon showers, direct electron pair production, and muon bremsstrahlung. Energy loss occurs in very small fractions of primary energy. In combination with relativistically extended decay length, this low loss rate allows muons to penetrate deep earth crust; instead, muons either decay or they captured by a nucleus causing another decay electron shower.

2.3 Radionuclides

In our environment there are three types of radionuclides: primordial, cosmogenic and anthropogenic.

Regarding primordial radionuclides, all nuclides that still exist since they were produced in stellar nucleosynthesis are called primordial; ^{40}K, ^{232}Th, ^{235}U, ^{238}U, latter three are starting nuclides of three naturally occurring decay chains, belong to this group. Furthermore, there're some elements with primordial radioisotopes (i.e., ^{87}Rb, ^{113}Cd, ^{115}In, ^{190}Pt, ^{144}Nd, ^{176}Lu, ^{138}La and others), but they're only relevant as a background source in very specific cases. Elemental abundance of Th and U in Earth's crust is very variable and different average values have been determined, which are for Th in range (17-60) Bq/Kg and for U in range (16-110) Bq/Kg. All their decay products are present in materials as well, unless chemical or physical separation will take place. ^{40}K is also present everywhere: living beings contain a very large amount of potassium, also food and vegetation are great storers of potassium; its concentration varies very much from levels of hundreds to thousands of Bq/kg as in soil samples down to tenths of mBq or even less in pure materials like copper, lead and special plastic products. It's often considered as less problematic as it can rather easily be identified but nevertheless, in some cases its presence can be limiting to the experimental sensitivity.

About cosmogenic radionuclides, they are produced by interaction with matter of secondary and tertiary cosmic ray particles [22] i.e., ^{3}H, ^{14}C, ^{7}Be through interactions in upper atmosphere between high energy cosmic ray particles and oxygen and nitrogen. Their production rate is approximately constant and high amount is present in atmosphere and in living animals and plants. Also, they're many more radionuclides which are produced by neutron and muon capture from cosmic radiation in atmosphere (i.e., ^{108m}Ag, ^{110m}Ag, ^{57}Co, ^{58}Co, ^{60}Co).

Describing anthropogenic radionuclides, they're man-made radionuclides produced by nuclear reactions either in nuclear power and reprocessing plants, nuclear weapons testing, production of radioactive sources for industrial and medical applications. Radionuclides belonging to this group are ^{60}Co, ^{137}Cs, ^{238}Pu, ^{241}Am. They're present in environment, because they're and were freed either in nuclear incidents, in nuclear weapons testing and as emission from reprocessing plants.

All these radionuclides are found in decay chains, where activities of all product nuclides are equal to activity of their respective parent nuclides; secular equilibrium is rarely achieved in most surface and near-surface geological environments. A special case is referring to Rn because it could escape from materials either by recoil on ejection of alfa particle or by diffusion. Longer-living progeny of Rn is ^{210}Pb, it's readily attached to aerosols and finally deposited on surface by washout and dry deposition. Since Rn derives from decay chains of Th and U, higher concentrations of them require a thicker shield against gamma-radiation; furthermore, they cause higher levels of Rn and neutrons.

Focusing on lead, ^{210}Pb is a natural radioactive isotope and a decay product of ^{238}U found in natural environment along with ^{222}Rn and ^{210}Po. Its contribution to internal exposure of man through ingestion is 20% but represents 70% of internal exposure of man through inhalation due to Th and U decay chains [23], fig 3.

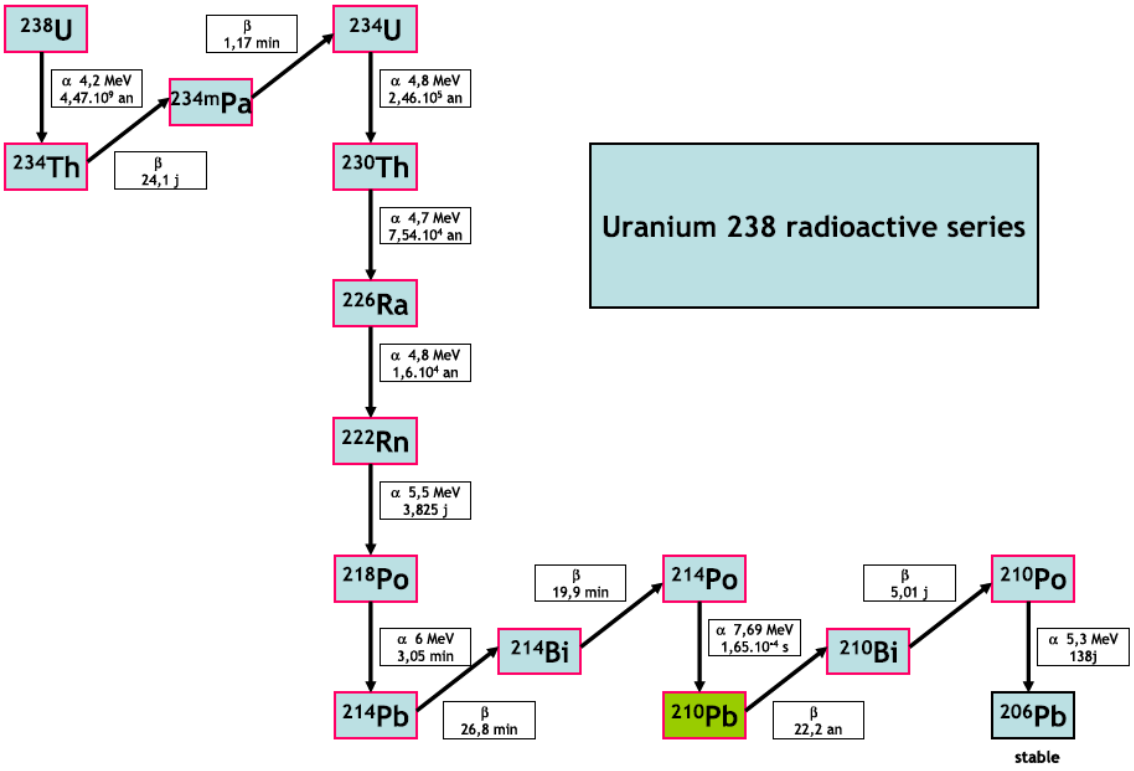

Fig. 3 ^{238}U natural radioactive series

Regards materials involved in physics experiments, ^{210}Pb is an isotope to always monitor to know its amount; it has been found that in common materials adopted in setup of experiments, an important radioactive contribution is due to presence of ^{210}Pb and its product nuclide ^{210}Bi and ^{210}Po. Having a long half-life (^{210}Pb $t_{1/2}$=22 yr), its abundance and also related to its product nuclides could be higher than expected from secular equilibrium chain.

About radon, it's a natural and relatively short-lived radioactive inert gas and it's produced in radioactive decay of radium, especially ^{222}Rn in ^{226}Ra decay (^{238}U decay chain), ^{220}Rn in ^{224}Ra decay (^{232}Th decay chain) and ^{219}Rn in ^{223}Ra decay (^{235}U decay chain). Half-life of ^{220}Rn ($t_{1/2}$=55.6 s) is shorter than ^{219}Rn ($t_{1/2}$=3.96 s) [24]. Nevertheless, ^{220}Rn is more sensitive to barometric pressure changes and other factors influencing emanation; although this isotope is present with same or higher activity in rocks, soil and building materials, its concentration in air is normally below level of ^{222}Rn. ^{220}Rn presence strongly decreases with

distance from emanating walls owing to its much smaller diffusion length during lifetime, ^{219}Rn is negligible in most low radioactivity background considerations.

Regards to air, concentrations of ^{220}Rn and ^{219}Rn can be ignored compared with concentrations of ^{222}Rn and its product nuclides, for this reason ^{222}Rn has major background contribution of natural radiation [25,26].

Precipitation of ^{222}Rn from surface into atmosphere [27], also exhalation rate is affected by various environmental and meteorological parameters [28–30]. This concentration into air affects daily monitoring of environmental gamma dose and it has a great impact on alarm accuracy of radioactive emergency monitoring of nuclear facilities causing increase of difficulty related to nuclear emergency screening [31,32].

2.4 Radio-impurities

Focusing on radio-impurities, presence of radionuclides in raw materials can affect eventual application of final products, due to presence of principal contaminants as ^{40}K, ^{232}Th, ^{238}U. Different processes can introduce contaminations level not always acceptable for material used in low radioactivity experiment, during industrial processes could be several steps with easy possibility to contaminate them.

Decay product nuclides coming from ^{232}Th and ^{238}U decay chains can have long decay times, therefore they cannot be overlooked; some of these elements are ^{230}Th, ^{226}Ra, ^{210}Pb, ^{228}Th and their progenies.

In metallic materials, there're different levels of contamination depending on each material, copper is generally high purity due to its high potential redox (0.337 V) compared to Th, U, K and their product nuclides; it's routinely purified after smelting by electrolytical dissolution and redeposition in solution even in large-scale production, so it's separated from all radionuclides in environment. Instead, lead and tin usually involve formation of waste mainly composed by iron silicates after smelting process and this waste takes up lithophile elements. High concentration of Si, Al, O, some metal of 1st group and transitions

metals can be found in this slag; thus K, Th and U are concentrated in waste. Production of Fe and Al is more difficult because higher reductive conditions are need during smelting process, due to greater dissolution of elements already presents in earth's crust into metal phase. Purification of Th and U become more difficult and expansive, generally these metals are less used than copper. Lastly, aluminum is normally strongly contaminated with Th and U but depleted in ^{226}Ra ^{228}Ra, so it's common to find very pure Al commercially.

A completely different behaviour is shown by plastic materials, most plastics consist mainly of C, H, O, so major impurities is due to ^{14}C and tritium; during chemical processes, it's easy to use starting materials containing very low amount of tritium and ^{14}C, on this way contamination risk is reduced to lower levels. Nevertheless, contaminations could come from inorganic additives, catalysts, mechanical machining, etc.; however, by purification methods (i.e., distillation, crystallization, melting) it's possible to obtain radiopure materials.

Focusing on other materials, tungsten and tantalum find few applications in physics experiments due to their limited availability. Mercury has a high radiopurity that it can be even further enhanced by continuous distillation, its longer-living radioisotopes ^{194}Hg is produced in wide quantities by exposure to high-energy neutrons; however, Hg requires a container whose radiopurity is more difficult to control. Fe is cheaper than Hg, it's usually contaminated with ^{60}Co coming from furnace linings.

3 Low background techniques

The background reduction in underground experiments strongly depends on the material selection. Both the shieldings passive materials (lead, copper, polyethylene) and the detector active materials (germanium, sodium iodine) must undergo careful selection and cleaning protocols. In this chapter the most common techniques for material screening are introduced, in particular the ICP-MS on which this thesis focuses.

3.1 Material treatment

Material selection is most fundamental prerequisite in low radioactivity experiments. During assembly of detector and handling samples, surface contamination is a factor to be kept under monitoring. Anyway, materials washing is previously required to optimize procedures, often using surfactants or dilute solutions of high purity acids. Common acids are HNO_3, HF, HCl, rarely H_3PO_4; however, especially in case of ICP-MS characterization, it's important to remove acid traces after washing. The main problem is related to interferences due to presence of HF and HCl, as well as etching quart components in case of HF.

Moreover, even mechanical processes especially on metal samples (i.e., welding, drilling, incisions) can release contaminations giving problems during measurements phase; therefore washing must be carefully done, subsequently also drying of materials is very important.

3.2 Screening techniques

Nowadays, available methods to characterize materials are the following:

- γ-spectrometry: non-destructive method identifies and/or quantifies radionuclides, regards to their decay chains, by analysis of γ-ray energy spectrum produced in a spectrometer; energy of incident γ-ray is measured by detectors, built with high radiopure materials to create efficient shielding.
- Mass spectrometry: in Glow-Discharge Mass Spectrometry (GD-MS) solid samples are sputtered in a low-pressure direct current argon discharge, sputtered atoms are

ionized in this plasma and extracted into the mass spectrometer for separation and detection. Otherwise, in Inductively Coupled Plasma Mass Spectrometry (ICP-MS) most of elements of periodic table are detected at milligram and nanogram level per kilogram; application fields are wide, as environmental monitoring, geochemical analysis, metallurgy, pharmaceutical analysis, clinical research.

- Neutron activation analysis: an analytical technique that relies on measurement of gamma-rays emitted from sample previously irradiate by neutrons; rate of which gamma-rays are emitted from an element in sample is directly proportional to concentration of that element [116]. Sensitivity in range 10^{-10} – 10^{-12} g/g for Th, U, K depends strongly on sample matrix.
- Liquid scintillation counting (LSC) allows to measure low-energy contaminants as ^{14}C and ^{3}H, determination of background is depending on primordial contamination in phototube; range of sensitivity for LSC commercial counting is from mBq/Kg to Bq/Kg.
- Rn-emanation: escape of radon atom from Ra-bearing grain into pore spaces; number of radon atoms released per number of radon atoms generated is known as emanation fraction, emanation coefficient or emanation power, etc [117].
- ^{226}Ra measurement is related to U chain, infact the best way to measure this isotope is through ^{222}Rn; this isotope is extracted from any large quantity of material, collected on charcoal and measured in various types of sensitive Rn detectors.
- α-spectrometry: a radiometric analytical technique for qualitative identification and quantitative determination of α-emitting radionuclides in environmental, biological and nuclear technology related samples [118]; modern α -spectrometry with Si detectors yields high-energy resolution and a low background. Sensitivity is limited by thin source layer required to maintain good energy resolution, this technique and chemical extraction procedure result in sensitivity ranges of 1-100 mBq/kg for Th and U.

ICP-MS and gamma-ray spectrometry will be more in detail discussed below.

3.3 Gamma-ray spectrometry

Gamma-ray spectrometry is a technique to perform quantitative and qualitative analysis of radionuclides, based on detection of gamma-radiation emitted during their decay processes; a wide use is performed in monitoring of radioactive substances in environment as many natural radionuclides and produced by nuclear processes emit gamma-radiation. One of its peculiarities is related to the ability to simultaneously detect activity of several radionuclides with a single measurement; range of interest for gamma-emitting radionuclides is 30 – 2000 keV.

As shown in fig. 6, gamma-spectrometer is composed by few components as detector, detector shielding, electronic unit, computer with dedicated software.

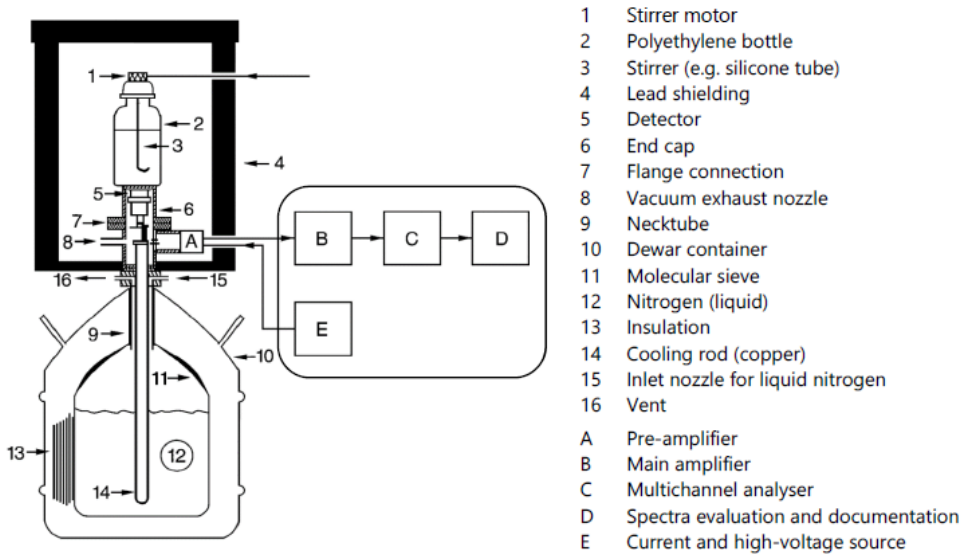

Fig. 6 Schematic design of a gamma-spectrometer

Regarding detectors, different materials can be used for this component, each with different characteristics:

- NaI(Tl) and $LaBr_3$ are commonly used for screening procedures, in mobile measurement systems and dose rate measurements;
- Si(Li) for determine activity of X-ray and low-energy γ-ray with energies below 60 keV;

- HPGe is specific for radioactive substance due to their high energy resolution, two types of detectors are available: p-type germanium that his doped with trivalent element as boron, and n-type germanium doped with pentavalent elements as phosphor.

Also regard to crystals, their geometry has different shapes (planar, coaxial, special forms) thus varying their efficiency; for material screening, it's wide important must be evaluated best crystal-sample relationship. Focusing on HPGe crystals, high voltage is necessary for their activity as well as very low T; to ensure a long thermal stability, use of permanent cooling is carried out since to reduces changes in its dead layer due to diffusion.

Some important parameters for detectors to take into consideration are related to sensitivity, energy resolution capability and peak-to-Compton ratio; they're determined for gamma-radiation emitted by ^{60}Co at 1332.5 keV, these parameters are certified as standard data for detectors. Sensitivity is defined as ratio of efficiency of detector considered to that of a reference detector stated in % [119]. Full width at half maximum of ^{60}Co gamma peak is used to determine energy resolution.

Regards measurements to be carried out, some characteristics of individual detector must be evaluated, such as: number of samples, sample matrix, geometry of counting source, energy region of emitted photons, detector properties. If it's possible, the choice of detector affects possibility to locate largest amount of sample, high energy resolution capability and high peak-Compton ratio.

Minimization of environmental radiation is very important to ensure high performance of detectors, especially about shielding taking into account intrinsic radioactivity of materials; several materials can be used for shielding as steel, cadmium, copper and mostly lead. Impurities inside materials should be as low as possible (i.e., ^{210}Pb in lead, ^{60}Co in steel), as they can affect measurement by altering results. Short lead thickness (~ 10-15 cm) is able to suppress peak of ^{40}K for low-level measurement systems, furthermore in this purpose lead that's used must be depleted of ^{210}Pb as much as possible.

Gamma-radiation generates X-ray fluorescence close to 75 keV coming from lead shielding, a coating based on a material with lower atomic number (i.e., Cd, Cu) is used to absorb this radiation. Furthermore, since radon is in the air, it's detected in spectrum through its decay products covering all other peaks in same region of interest. Using a continuous nitrogen flow starting from dewar via hose system, it's possible to expel radon from shielding [120–122].

3.4 Inductively Coupled Plasma Mass Spectrometry

Inductively Coupled Plasma Mass Spectrometry (ICP-MS) has become one of the most successful methods in many analytical laboratories for accurate and precise trace element, isotopic determination, short analysis time, possibility to check several elements at the same time. Various types of ICP-MS instruments is commercially available, providing several pros and cons for specific applications. Many similar components are present in mass spectrometers (i.e., nebulizer, spray chamber, plasma torch, interface and detector); they principally differ regard design of mass analyzers. Summarily, inductively coupled plasma mass spectrometer can be subdivided in following parts (fig 7): sample introduction, ion source, ion extraction, ion separation, ion detection [123].

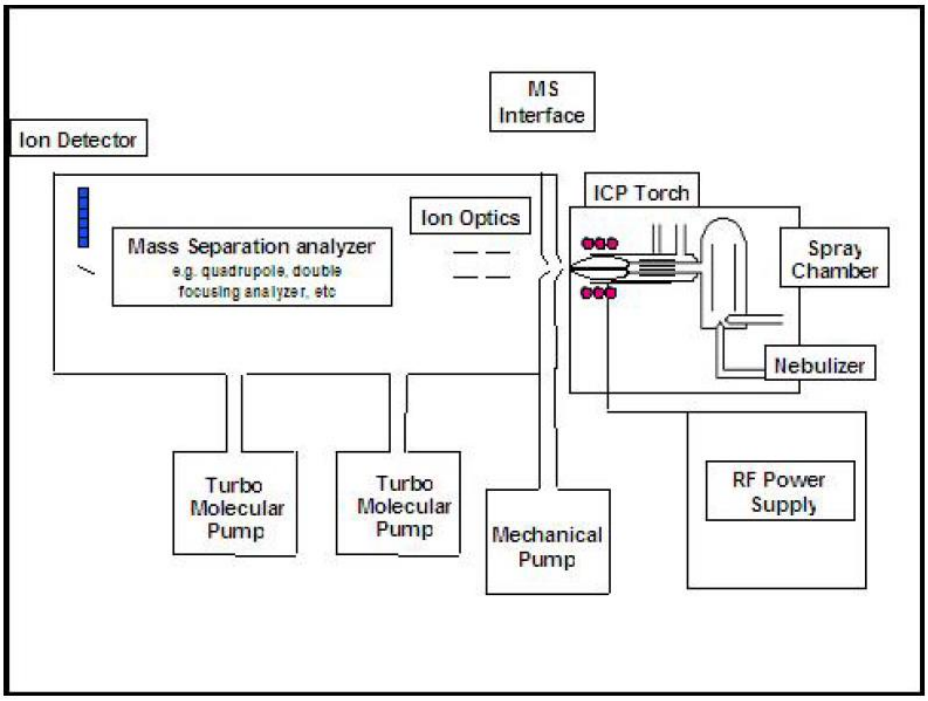

Fig. 7 Schematic drawing of ICP-MS

3.4.1 Sample introduction system

This type of instrumentation can measure solutions coming from different devices [124]; liquids are dispersed into fine aerosols using various type of nebulizers and using Ar as carrier gas to allow sample introduction into mass spectrometer, as shown in fig. 8.

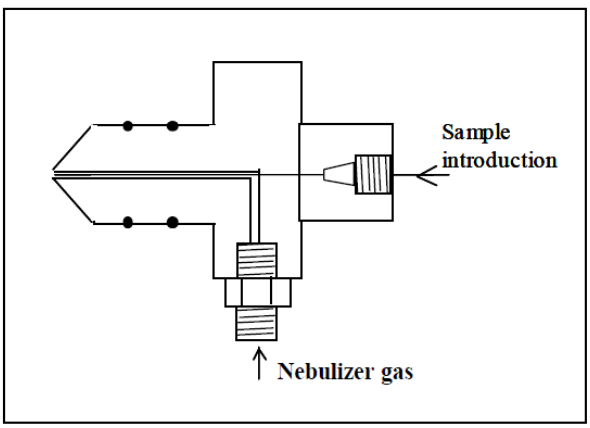

Fig. 8 Schematic arrangements of a micro-concentric nebulizer

A common type of sample introduction devices used for ICP spectrometry is pneumatic nebulizers, two basic configurations are referred to this system:

- concentric type
- crossflow type

Regards to concentric type (i.e., Micromist) sample solution passes through a capillary surrounded by a high velocity gas flow parallel to capillary axis; crossflow type nebulizer has a liquid-carrying capillary at 90°C to tube carrying high-velocity gas stream. A broad and more detailed description of nebulizers is present in literature, taking into consideration that each nebulizer is recommended for some types of matrices [123–125].

For solid sample introduction system, in ICP-MS an optimum approach is LA-ICP-MS [126–129]: a process of removing material from a solid surface by irradiating it with a CO_2 or Nd/YAG laser beam. At low laser flux, material is heated by absorbed laser energy and evaporates or sublimates; differently, at high laser flux, material is typically converted to plasma.

3.4.2 Ion generation

During the nebulization process, fine aerosol droplets can represent nearly of 100% of sample depending on nebulizer type. Aerosol introduced into ICP-MS consists in plasma form, whose atoms are present in ionized state. Basic setup of torch consists of three concentric tubes to support plasma with cool gas, auxiliary gas and carrier gas; torch is placed within a water-cooled coil, cooling performing by chiller plant, fig 9. As a flowing gas is introduced into torch, RF field is activated and gas in coil region is made electrically conductive by introducing a spark (plasma ignition). After spark-initiated ignition plasma is formed as result of snowball-like increase in number of ionized species in RF-field. Formation of plasma is dependent upon an adequate magnetic field strength and the pattern of gas streams follows a particular rotationally symmetrically pattern. Plasma is maintained by inductive energy coupling to flowing gases, to prevent possible short-circuiting as well as melting of torch, plasma must be thermally insulated from rest of instrument, this "insulating screen” is achieved by applying a cool gas flow between inner side of plasma and

other tube of torch at a relatively high flow rate. Argon gas is used for both sample gas and carrier gas, chemical species are decomposed into their atomic constitutes and also ionized with high degree ionization and low fraction of multiply charged ions [130].

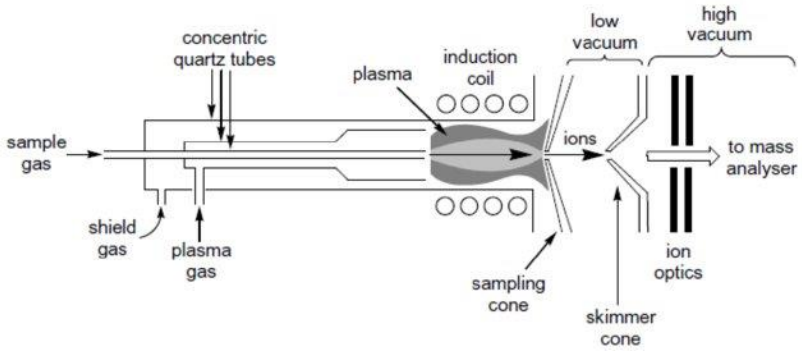

Fig. 9 Torch and interface region of typical ICP-MS instrument

Plasma acts as a reservoir of energy provided by RF field and transfers energy to analyte, various ionization processes have been suggested resulting from presence of species that are obtained during plasma generation; major species are not only Ar ions (Ar^+) and electrons (e^-), but also excited Ar* and argon metastable (^mAr) atoms. Different atoms require different ionization energies, such as difference can be successfully applied for improving analytes in comparison to interferences by tuning of RF power for analyte ionization; it's possible to partially separate interfering isotopes or molecules.

3.4.3 Ion extraction

Product ions in plasma are extracted and directed into mass spectrometer through interface region consisting of two cones (i.e., Ni cones, Pt cones), they are placed sequentially after torch, first is dedicated sampler cone and next is skimmer cone. Ion extraction in interface region is the most critical part of ICP-MS because ions must be extracted from plasma where they are at atmospheric pressure to mass spectrometer analyzer region at high vacuum (~ 10^{-7} Pa). In ICP-MS instruments, photons emitted by excited argon atoms result in high background signal reaching detector. To minimize

background, a so-called photon-stop is used in many quadrupoles based ICP-MS instruments [131,132], as a small metal plate placed in centre of ion beam, in order to prevent photons from reaching detector.

Positive ions are guided around photon-stop by positively charged cylinder lenses, or through a defined angle or off-axis les stack which also prevents photons from reaching detector. Regards to double focusing ICP mass spectrometers background contributions from photons are significantly reduced due to specific geometry of mass separation system.

3.4.4 Reaction/collision cells

Application of target gas in inorganic mass spectrometry was proposed by Becker and Dietze in 1983 [133] for background reduction and improving sensitivity in isotopic and trace analysis, concerning on dissociation of interfering molecule ions. Introduction of collision gas into multipole was found to be useful for improving ion focusing due to a decrease in ion kinetic energy and for reducing free ion's paths compared to dimensions of multipole, studying performance of three-dimensional quadrupole ion trap [134]; analogue effect called "collisional focusing" has been found for linear quadrupole ion guide [135,136].

It's also possible to use gas-phase ion molecule chemistry for neutralization or fragmentation of interfering atomic or molecular ions. Most abundant interferences in ICP-MS are usually caused by argon-based molecular ions (Ar^+ and ArX^+, with X as Ar, O, Cl, C, N and so other elements) [137].

Using collision cell ICP-MS, unwanted ions can be removed while operating under normal plasma conditions: collision cells based ICP-MS instruments offer limits of detection of less than $1*10^{-12}$ g/g for elements such as Pb, In, Sr; instead regarding to Fe, Ca, K, Cr, Se and As, detection limits of approximately $10*10^{-12}$ g/g are reported in literature [138].

Kinetic energy of ion can be reduced about 1 eV by collision with helium atoms resulting in better abundance sensitivity, this approach is much more effective than for instance increasing quadrupole mass spectrometer resolution, which would have a

significantly lower influence on abundance sensitivity. Helium introduction in collision cell leads a peak-tailing reduction of high-abundant isotope up to 3 orders of magnitude depending on considered mass [139].

Physical features of collision/reaction cells include number, length, diameter and spacing of RF multipole rods, length, and location of rods relative to gas filled cell, position and orientation of cell within instrument; use of additional RF/DC fields to supplement functions of main multipole ion guiding field, and design of ion injection/extraction optics [140].

Several ICP-MS developments have introduced in commercial instruments that use quadrupoles, hexapoles, octapoles to serve as reaction/collision cell and to provide confining fields for ion focusing and guiding. Main use is to prevent neutral species from ICP mass spectrometer (Ar metastable ions) from transforming into inevitable charged species which could reach the detector, where they might otherwise create new, potentially interfering ions, non-mass-resolved backgrounds signals, or detector noise [141].

3.4.5 Mass analyzers

3.4.5.1 Quadrupole analyzer

Ion's selection takes place through use of specific extraction lenses, generated beam is sent towards mass analyzer to perform mass separation, this area is under vacuum at ~ 10^{-6} Pa. Common mass separation devices are quadrupole analyzer, triple quadrupole analyzer and double focusing analyzer [142].

Regards to quadrupole analyzers, they're very common in commercial spectrometers due to their relative low cost and fast separation m/z; small changes in operating conditions can significantly alter ion transmission into analyzer, mass resolution is low comparing to other configurations (m/Δm=300). Layout of quadrupole mass analyzer is shown in fig. 10, four rods should have a hyperbolic profile to generate most stable electric field distribution;

many systems are manufactured using round rods with an interelectrode spacing to produce best approximation to optimum hyperbolic field [143].

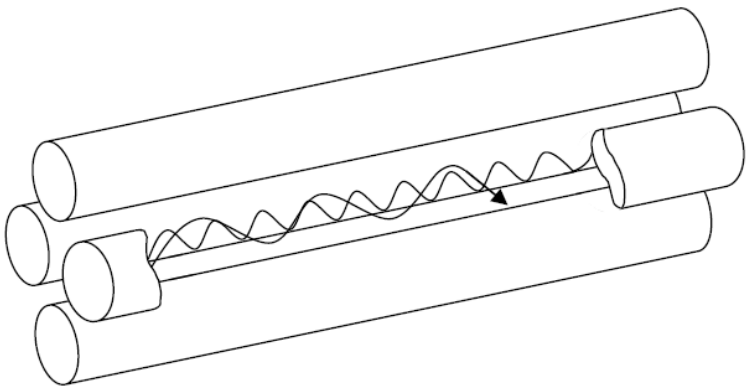

Fig. 10 Schematic of quadrupole mass analyzer with cylindrical rods

Potential in quadrupole field may be discussed by following equation [144]:

$$V = \frac{V_0}{r_0^2}(x^2 - y^2)$$

where V_0 is voltage applied to each rod, and parameter r_0 is half distance between opposite rods; electric field components in x, y, z directions are therefore [145]:

$$E_x = -\frac{dV}{dx} = -\frac{2V_0 x}{r_0^2}$$

$$E_y = -\frac{dV}{dy} = -\frac{2V_0 y}{r_0^2}$$

$$E_z = -\frac{dV}{dz} = 0$$

3.4.5.2 Double focusing mass analyzer

Regards to double focusing analyzers, it's important to consider interferences that can directly limit quantification of some elements; knowing radius of magnetic sector field r as well as widths of entrance and exit slits, it's possible to calculate maximal admittable mass resolution of magnetic sector field instrument, fig. 11.

Reducing energy dispersion of extracted ions, it's possible to improve mass resolution of instrument through a combination between magnetic and electrostatic field. Resulting ion trajectory deviation from energy dispersion in an electrostatic analyzer is opposite than in magnetic sector, energy dispersion effects in both type of analyzers will compensate each other; so that finally energy dispersion of ions doesn't change their focusing point.

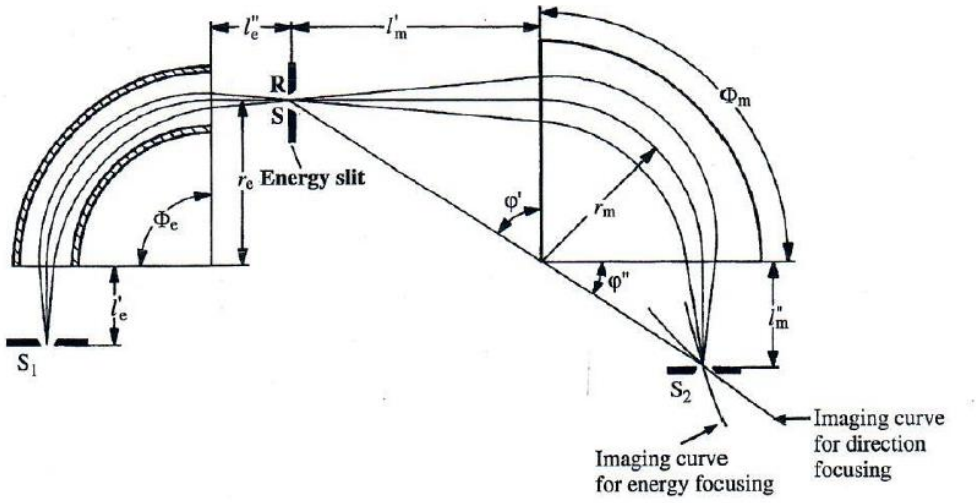

Fig. 11 Double-focusing mass spectrometry with Nier-Johnson geometry

In this picture, a double focusing sector is represented with two 90° sector fields: a cylindrical condenser and a magnetic sector field with deflection of ions in same direction and energy focusing; ion beams enter electrical and magnetic sector fields vertically. By a defined deflection radius of electric sector field r_e and magnetic sector field r_m respectively, energy and directional focusing of separated ions beams at one position on imaging curve is achieved. Exit slit S_2 is installed at this point of imaging curve for energy focusing and imaging

curve for direction focusing of ions. Through a variation of magnetic field B ions of different masses can be transferred under double-focusing conditions at defined deflection radius rm and can be detected one after other. This configuration of mass spectrometer permits a large divergence angle and second order directional focusing.

Double focusing is also possible by combination of two sector fields with opposite velocity dispersion, if deflection of ions in both sector fields is opposite; a typical instrument is shown in fig. 12.

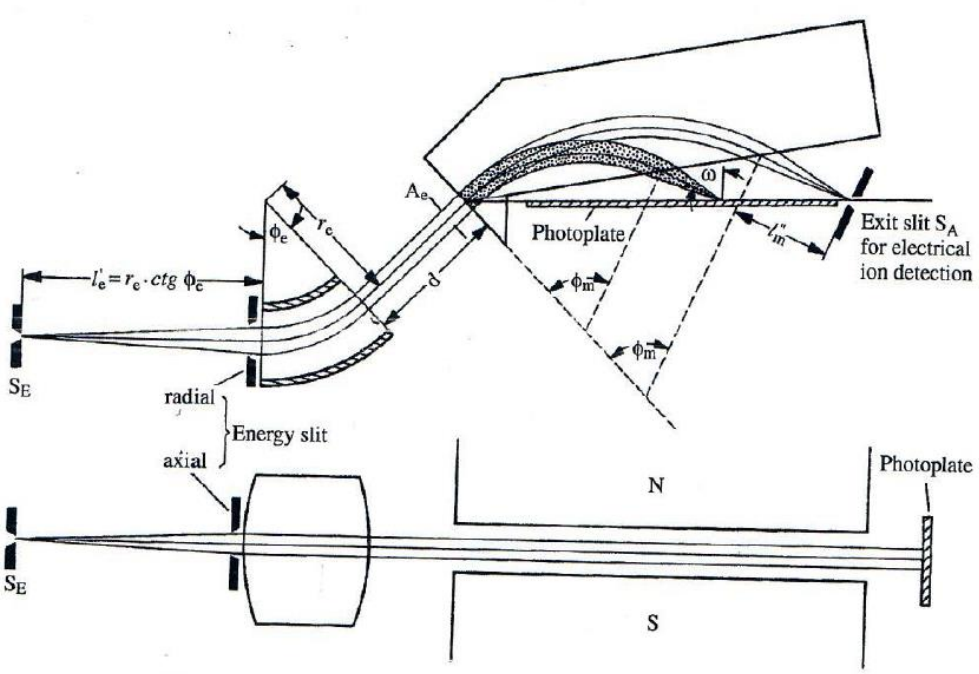

Fig. 12 Schematic of double-focusing mass spectrograph with Matthau-Herzog geometry with a linear imaging curve

A linear focal plane consisting of an electrostatic sector field for energy focusing of ion beam, followed by a magnetic sector field which deflects ions in opposite direction; ion optics produce an image of entrance slit (S_e) for each ion species of different mass whereby all images of separated ion beams are situated on a straight line. Due to this property, nowadays ion detectors mostly used are ion sensitive photo-plate, focal plane array

detectors or multiple microchannel plates, according to mass-to-charge ratio and energy-to-charge ratio. Ion sensitive photographic plate has been used for many years for sensitive and quasi-simultaneous detection of separated ion beams over a wide mass range. It's advantageous that by using a photographic plate for registration of ions, mass resolution (R) is constant along whole photographic plate; an aperture slit between electric and magnetic sector field (A_e) selects a small range of broad energy spectrum ions.

3.4.6 Ion detection

Ion beam separated by mass analyzer is converted to electrical signal using various detectors, in mass spectrometers is widely used secondary electron multiplier (SEM); it's a fast detector of positively charged ions, also electrons and photons can be detected by this system. Regards to principle operating, positive ions impinge upon the first plate, or conversion dynode, resulting formation of secondary electrons; in SEM detector, positive ion current is converted into an electron current at conversion dynode. Ejected secondary electrons are accelerated and impinge on surface of second dynode whereby generated again a multitude of secondary electrons; to obtain a high yield of secondary electrons from implanted ions, dynodes are connected to successively higher positive potentials. Effectiveness of remaining stages of electron multiplier depends upon geometry of plates, interstage voltage, material, and stage of activation of plates and degree of magnetic shielding [146].

SEM operates as an "open ion detector" inserted into ultra-high vacuum of any mass spectrometer either in current amplification or ion counting mode. Operation mode depends on magnitude of high voltage applied to device, SEM operates in a medium amplification range with a gain 10^3-10^5, then resulting current at output can be measured in an analogue mode with conventional amplification techniques, fig. 13. At higher amplification (10^6-10^8), gain is large enough that individual electron pulses to be readily detected and counted using sensitive pulse counting electronics [147].

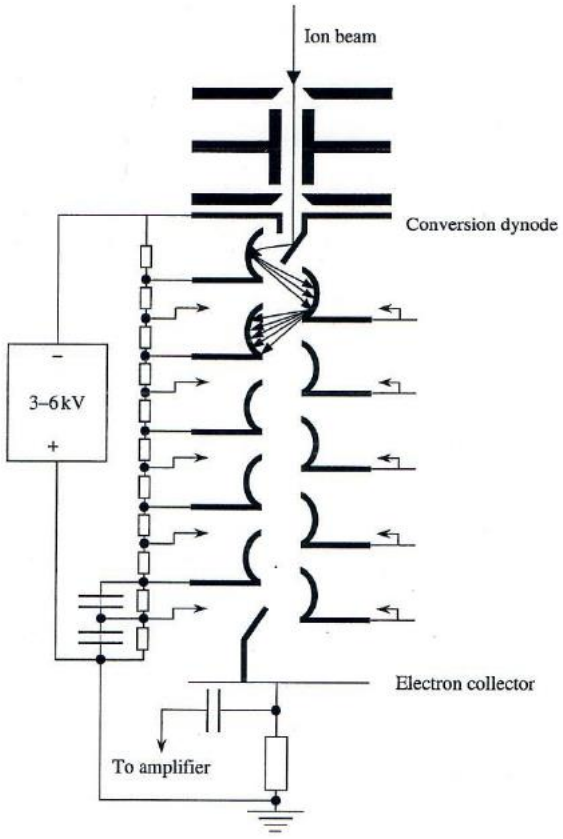

Fig. 13 Basic principles of secondary electron multiplier (SEM)

A possibility is to extend dynamic range of mass spectrometer employed up to 10^9 is regards application of dual ion detector mode; first detector section operates in analoug mode always active, second detector section provided additional gain to signale and it's used in pulse-counting mode. A sort of scheme is show in fig. 14.

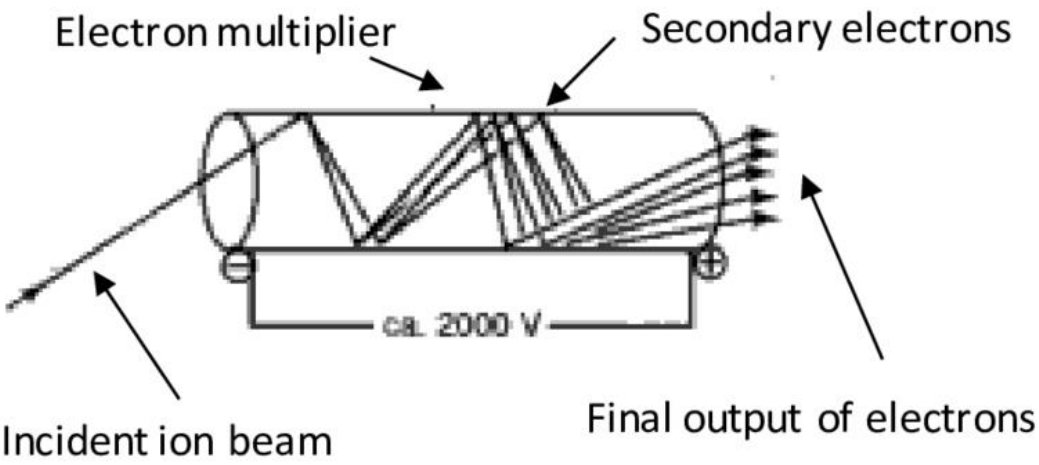

Fig. 14 Schematic of dual ion detector mode

New type of SEM with dual detector mode and high-speed amplifier operates in analogue mode for higher ion currents and in pulse counting mode for lower ions. Such a dual ion detector and permits mass independent cross calibration and allows mass spectrometric measurements on dynamic range to be extended up to nine orders of magnitude, concentrations from $1*10^{-12}$ g/g up to $1000*10^{-6}$ g/g can be measured by ICP mass spectrometer.

3.4.7 High resolution ICP-MS

Regards to High Resolution ICP-MS, one of most important characteristics is combination of magnetic sector field with an electrostatic analyzer, this configuration is able to reach values of resolution power up to 10000. Some elements are interfered in low resolution by formation of polyatomic species due to presence of elements present inside source (i.e., K, Fe, Ca, Al), however, high resolution can resolve their interferences.

Configuration of magnetic and electrostatic sector is composed by a magnetic sector field (angle = 90°) which separates ions according to their m/z ratio, followed by an

electrostatic sector (angle = 90°); their function is to filter species according to their kinetic energy, not considering their ratio m/z [148].

Principle of magnetic sector analyzer is referring to charged particle passing through a magnetic field deflected by a proportional angle to mass and charge of particle; radius of curvature of deflection is dependent on both m/z ratio of ion and strength of applied magnetic field. A homogeneous magnetic field is generated by flat pole shoes positioned parallel to each other, so strength is the same at every point in the field z. Effect of accelerating voltage (V) is to drive ions entering in magnetic sector, then all energy is converted into kinetic energy of ions. Summarizing this phenomenon, an ion moving its mass (m) with defined velocity (v), this corresponding to number of electrons lost (z) by atom during ionization process with elementary charge e.

Electrostatic sector performs a separation of entering ions according to their energy content, there are two cylindrical condenser plates with opposite potentials, to which a grounded deflection voltage is applied roughly in the middle. Positive voltage is applied to outer plate of condenser and negative voltage is applied to inner one.

During pass of ions into electrostatic analyzer, they travel in a circular path of radius r, such that electrostatic force balances centrifugal force:

$$\frac{mv^2}{r}=\text{Eze}$$

as E electrostatic field strength. Radius of curvature r depends on energy of traveling ion and not on its mass. A broad energy distribution is reduced to a very narrow energy distribution, permitting higher resolution to be achieved.

About possibility to work in low, medium, and high resolution, work situation is following:

- low resolution (R=400)
- medium resolution (R=4000)
- high resolution (R=10000)

taking into great consideration that increasing of resolution corresponds to decreasing of sensitivity.

3.5 Gamma-ray spectrometry and ICP-MS: a complementary approach

Emphasizing advantages of ICP-MS, it's very important its possibility to measure very small mass of samples reaching high sensitivity; furthermore, radioactive contribution of different components inside same sample can be discriminated through different sample treatment. Otherwise, gamma-ray spectrometry has advantage of very easy sample handling, since no special preparations must be made beyond washing; measurement time depends on mass sample and impurities placed inside it, long time are required to reach high sensitivity.

Specifically, ICP-MS measures directly radionuclide with high sensitivity (precursor nuclide), while gamma-ray spectrometry measures product of decay chains (product nuclide) to check secular equilibrium; hese two techniques are in very good agreement when measuring natural radionuclides for very low concentrations (10^{-10} g/g in Th U), as they occur in in ultra-low background materials

ICP-MS is a destructive technique and chemical preparation of sample is required: mineralization and dissolution are critical processes, they must be performed with greatest care to avoid contamination from reagents, glassware, etc; another advantage of ICP-MS is referring to its capability to measure many samples derived from same or similar preparative chemical treatment, combined with a very small amount of sample mass necessary for analysis (grams or fraction).

Furthermore, gamma-ray spectrometry is non-destructive technique, samples were measured without chemical preparation and after acquisition it's possible to re-use them, it requires a large amount of sample (in the order of kg) and long-time of acquisition signals to get best sensitivity.

Summarizing, it's possible to affirm a good agreement between these two techniques for measure of natural radionuclide content in various type of material, they also give complementary information refer to radiopurity [149].

4 Material Purification and Screening at LNGS

Among the most common techniques for material screening the ICP-MS presents several advantages, first of all the versatility. In the framework of this thesis, this versatility has been exploited to respond to the growing needs of astroparticle physics experiments to understand and reduce the background due to radioactive contaminations. This chapter illustrates in detail the work carried out, reporting the methods adopted and the results obtained.

4.1 Germanium

Germanium is a semiconductor, and it was the first material to made into practical semiconductor devices, diodes, etc; an important issue regards mobility of holes, it's greater than silicon and any other common semiconductor. The holes and electrons mobilities are closer in germanium than other semiconductors, particularly at low temperatures [150]. Moreover, germanium is potentially enabling element of next-generation electronics and renewable energy applications. It was first isolated by Clemens Winkler in 1886 from mineral argyrodite (Ag_8GeS_6) [151]; with regards to Earth's crust, it's present in very low concentration (<< 0.5%) [152]. Always it's present as in impurity in minerals of other elements with common oxidation state +2 and most commonly +4 [153]. Very wide use is on various high-tech application, such as infrared systems, optical fibers, semiconductors, solar panel, polymer catalysis, etc, based on its chemical and physical properties.

Nowadays, main source of germanium is zinc refinery residues and fly ash, and thus its production increase depends on motivation of zinc refineries and coal power plants to engage in germanium market [154]. Criticality of germanium lies primarily on implementation of an efficient and profitable production process rather than resource availability [155].

Due to its high cost, purchasing of high purity germanium is often too expensive; to find a useful solution, process of metallic germanium purification could be a suitable way to perform in order to optimize costs and energies.

4.1.1 Enriched germanium sample

As already discuss into LEGEND paragraph (see below), germanium detectors are manufactured from ^{76}Ge, main reason for ^{76}Ge detectors use is their higher energy detection and efficiency and higher resolution [156].

Several steps are involved before germanium detectors production, like isotope enrichment, reduction of germanium dioxide to metal form, zone refinement, chemical purification and manufacturing waste containing enriched germanium into enriched and ultra-pure materials used in detectors for rare event experiments [157–159].

Isotope enrichment was performed by gas centrifuge enrichment process, involving fluorination of metallic ^{nat}Ge to gaseous $^{nat}GeF_4$; its enrichment passing through many centrifuges and its subsequent hydrolysis to obtain $^{76}GeO_2$. Drying and calcination are sequent steps to remove water and other impurities, reduction with H_2 will give enriched ^{76}Ge.

4.1.2 Zone refining technique

Zone refining (ZR) technique is a physical method for purifying metals. This technique was developed at Bell Telephone Laboratories in the early 1950s [160].

Increasing yield and reducing impurity content is principal aim of this process. This technology is based on deeply purifying metals [161]; distribution of impurity elements in solid and liquid phase of bulk metal melt is determined by thermodynamic properties of system. Melting point of metal can increase or decrease due to presence of trace impurities. Decreasing melting point causes solid solution to change from molten state to solid state, so impurities migrate from solid state to liquid phase; by increasing melting point opposite occurs.

Regards to high purity germanium single crystals, many applications can come from products obtained from zone refining in semi-conductor detectors industries, this material come from ZR. If it's conducted on a grown single crystal or on the interface of a single crystal

seed with an ingot, product process would be a single crystal and the process called “zone melting” fig 15. Zone melting is also considered as a technique to grow single crystals [162].

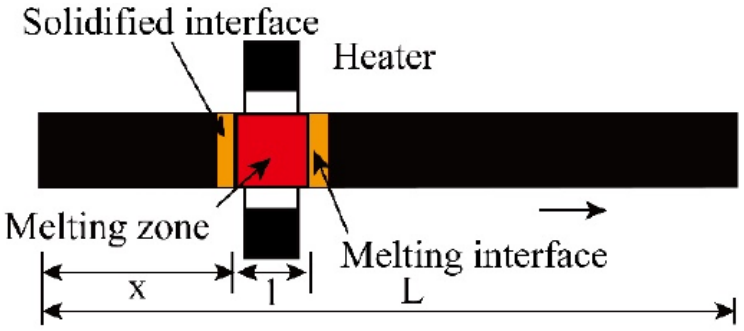

Fig. 15 Process of single-pass zone refining

Specific process involves metal material placed in tubular furnace and a movable heating ring outside tube; initial concentration of impurities in metal ingot is locally melted into melting zone, then slowly mode heating ring to right. Melting zone also slowly moves from left end to right end, melted metal gradually solidifies again; impurities precipitate at the top of melting zone, concentration of impurities distributed in liquid phase is greater than that in solid phase. Repeat of this process occurs many times, until impurities are deposited at both ends, purifying middle part of ingot.

Using multi-melting zone refining shown in fig. 16, one advantage is simultaneous melting of multiple zones of ingot; impurities don’t diffuse in solid phase, but mass transfer rate in liquid phase is very fast, so concentration of impurities in liquid phase is uniform [163,164].

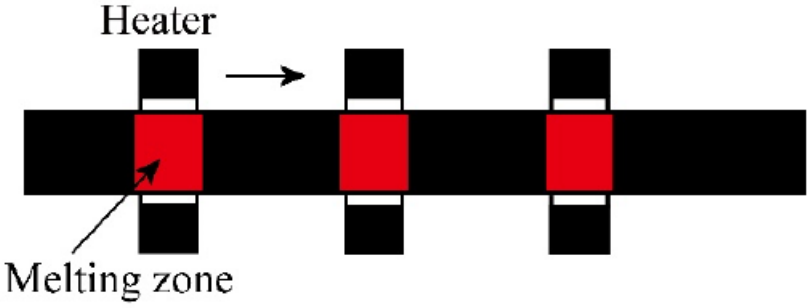

Fig. 16 Process of multi-pass melting zone refining

After multiple zone-refining passes, the purest central section can directly used for germanium crystal growth by Czochralski method [165].

4.1.3 Experimental section

4.1.3.1 Purification Ge samples

Ends of ingot (head and tail, kerf) coming from ZR are cut off and subjected to a chemical purification performed at LNGS, where a chemical plant has been designed and built to fit this purpose.

Schematic purification process is composed by chlorination (from metallic Ge to $GeCl_4$), fractional distillation, hydrolysis (from GeO_2 to GeO_2*nH_2O) filtration and calcination (GeO_2 purified), fig 17.

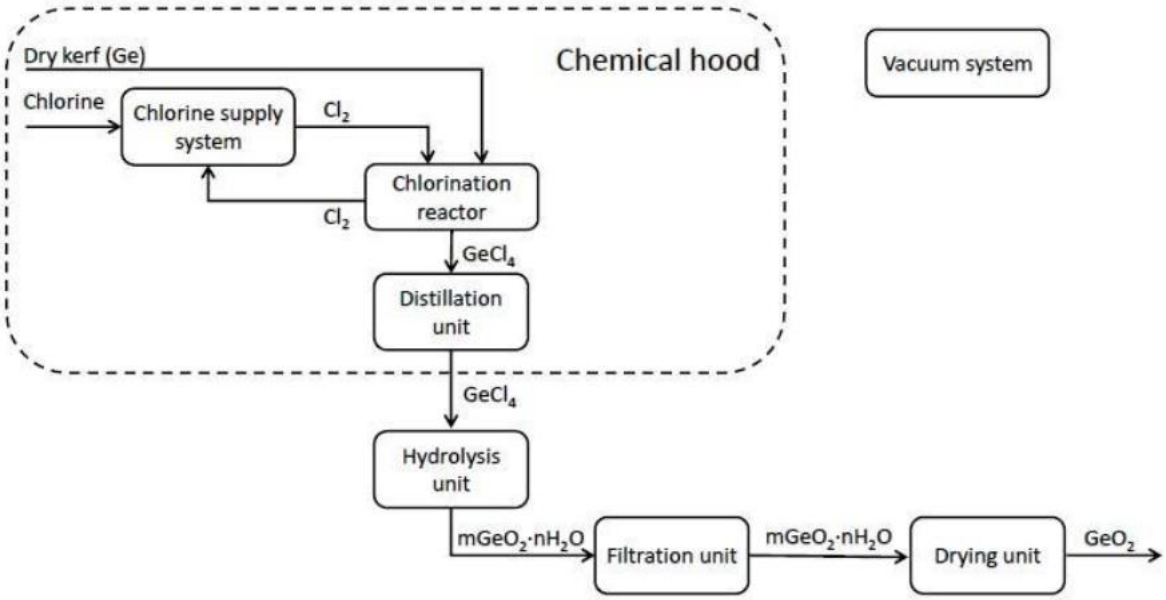

Fig. 17 Schematic diagram of purification process

The main procedure is distillation, as at high temperature germanium therefore it's necessary to transform solid sample into a liquid solution; first reaction that occurs concerns

chlorination of germanium samples, to make starting material more reactive and volatile in order to carry out distillation. At high temperature Cl-Cl bond cleavage takes place, so product will be $GeCl_4$, as reported in the following reactions:

$$^{76}Ge + 2Cl_2 \xrightarrow{400°C} {}^{76}GeCl_{4(l)}$$

Therefore, experimental procedure involves a quartz vessel with 500 g of germanium loaded and placed into a reactor to allow chlorination, temperature of 400°C is needed to formation of $GeCl_4$. During chlorination, $GeCl_4$ produced are collected into a column to sequent distillation; this process takes place until total reaction of Ge with Cl_2, experimental ratio Ge-Cl_2 is 1:4 to perform total conversion of germanium to $GeCl_4$.

During distillation, impurities keep stay in the bottom of column due to their higher boiling point, while distilled phase is condensed and collected in another column of same volume; many characterizations by ICP-MS were performed in real time to monitor progress of distillation and therefore to be able to decide when to stop it.

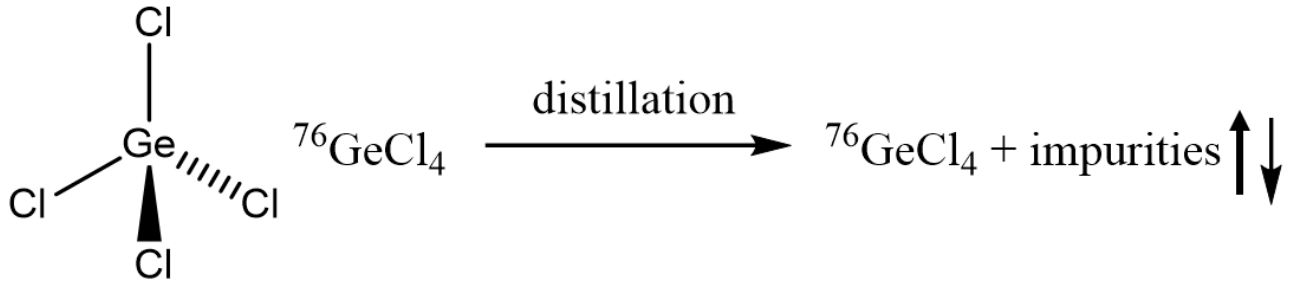

In Ge kerf, it's common to find traces of GeO_2 coming from previous process; an advantage of chlorination is the selective reaction with metal germanium and not with GeO_2. A possible explanation is based on bond-dissociation energy, Ge-Cl is 103 kcal/mol while Ge=O is 158 kcal/mol; for this reason, energy absorbed from chlorination is not enough sufficient to cleavage Ge=O bond, too high energy gap between reagent and product, fig. 18.

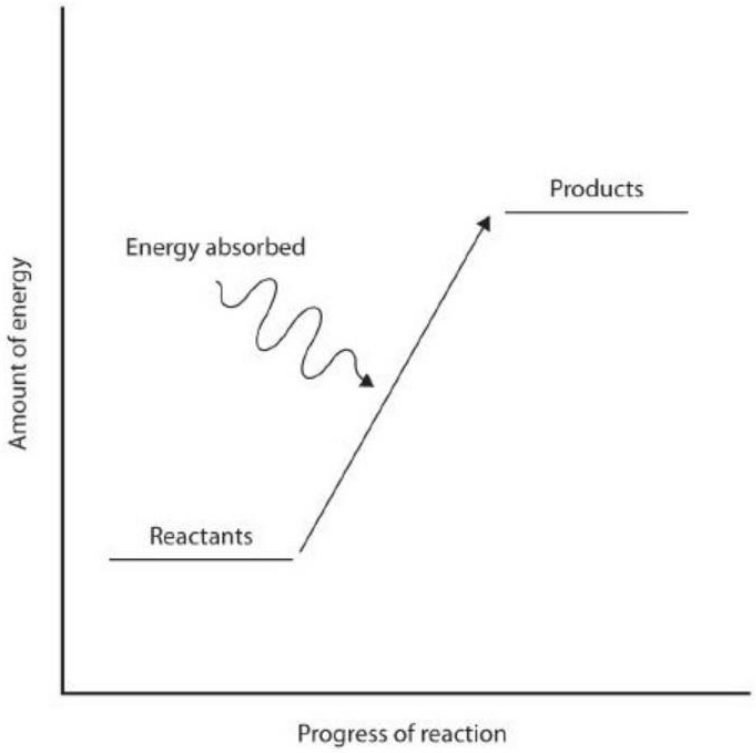

Fig. 18 General energy profile regards to chemical reaction

Chlorination is not able to break covalent bond Ge-O, so reaction of GeO_2 doesn't occur in chlorination process. Nevertheless, during reaction with Cl_2, GeO_2 can go into upper part of initial mass placed into vessel; thus, a sort of screen can be created preventing reaction between metal Ge and gaseous Cl_2.Due to this reason a reaction cannot be quantitative in presence of starting material composed by Ge/GeO_2.

Based on short analysis time of measurements, it was possibly taking decision about timing of purification in very short time (1-2 h). Moreover, chlorination and distillation processes could take place in parallel to save time.

Next step is hydrolysis, ultra-pure water largely reacts with $GeCl_4$ to obtain $GeO_2{*}(H_2O)_n$ with formation of HCl as reaction product; chemical trap captures and condenses formed HCl which is neutralized with NaOH.

$$^{76}GeCl_4 + H_2O \longrightarrow m^{76}GeO_2 * (H_2O)_n + mHCl$$

$GeO_2*(H_2O)_n$ is not soluble in water and therefore is found as precipitate; a way to follow to recovery is under-vacuum filtration to maximize elimination of excess water to obtain a white powder with the least amount of water.

Last step to be carried out is calcination to remove presence of water inside GeO_2 powder, a muffle is used to reach 700°C and keep it for 12 hours; on this way water is eliminated and GeO_2 dry is obtained as final product.

$$m^{76}GeO_2 * nH_2O \xrightarrow{\Delta T} {}^{76}GeO_2 * H_2O \uparrow$$

Characterization through ICP-MS was performed at the end of calcination step to check contaminants remains inside final products, GeO_2 powder with very low amount of impurities. A fundamental operation is store material just purified underground as soon as purification process gets completed in order to minimize its cosmogenic activation and production of undesired radionuclides like ^{68}Ge and ^{60}Co [159].

4.1.3.2 Technical considerations

Total reaction between metal Ge and Cl_2 is the main feature to take under consideration, regards to selectivity of this reaction; chlorination process only affects metal Ge, without interaction for GeO_2 placed in quartz vessel. A problem can occur during cutting of crystal related to presence of GeO_2, it's solved through this chemical step. Regards to safety, selective sensors for Cl_2 were adopted to check flow; chemical hood hosted purification plant to vacuum any produced fumes during process. Yield was estimated in the order of 98%. Distillation process was carried out by several cycles controlled by electronic counter, on this way it was possible estimate required time to convert total amount of $GeCl_4$.

Hydrolysis was proceeded in a quantitative manner, through continuous ultra-pure water flow under stirring; GeO_2 formation was immediate due to high reactivity of $GeCl_4$ with H_20, achieved yield was estimated in 97%. Subsequently, filtration was performed using a filter with very small holes in order to maximize separation; filtered products were placed into muffle at 700°C to remove water content present after last steps. Yield of entire process was estimated in 98%.

4.1.4 Materials and methods

Ultra-pure water (resistivity 18.2 MΩ/cm at 25°C) was obtained from a Milli-Q (Millipore Corporation, Billerica, Ma, USA), ultra-pure grade nitric acid was obtained from Hyper pure grade nitric acid (VWR Chemicals, Canada) using a sub-boiling distillation system (Milestone, Sorisole, BG, Italy).

The mass spectrometric analyses were performed using Agilent 7500a quadrupole mass spectrometer with an ASX500 autosampler from Cetac (Omaha, Ne, USA); the high-resolution double focusing Element2 mass spectrometer from Thermo Fisher Scientific, equipped with an ASX520 autosampler from Cetac (Omaha, NE, USA).

4.1.4.1 Mineralization of germanium samples

An aliquot of ^{76}Ge kerf was solubilized with mixture HNO_3/HF to perform solubilization, followed dilutions to obtain aqueous solution fit for purpose. Purity of all reagents and vials was previously checked by monitor of contamination through ICP-MS measurement, so it was carried out measure of blank.

About 20 mg of ^{76}Ge kerf sample was weighted and was solubilized with 250 µl HNO_3 UP and 100 µl HF in hot-block at 80°C for 1 hour, then solution has been diluted with ultra-pure water, the obtained dilution factor (DF) is into range 700-1000.

With regards on isotope analysis, the same preparation procedure used for semiquantitative analysis was adopted to mineralize sample, then obtained solution was diluted with DF about 100000 to perform isotope analysis.

4.1.4.2 Semiquantitative analysis

Samples shown in table 2 refer to starting material (Ge kerf), intermediate product ($GeCl_4$), final product (GeO_2) and Ge rest on quartz vessel at the end of process. About quantity, 1 g of metal Ge kept into vessel, starting from 500 g of Ge kerf.

Table 2 Samples list characterized by ICP-MS

Sample	weight [mg]	description
Ge sample 1B.1 TOP of METAL BAR	30.4	starting material
$GeCl_4$ Batch 1B.2 LIQUID	9.7	$GeCl_4$ after chlorination
$GeCl_4$ Batch 1B.3 LIQUID	11.7	$GeCl_4$ during distillation
GeO_2 Batch 1B.4 POWDER	3.4	GeO_2 final product
Ge sample 1B.5 vessel-rest	1.08	Ge kept into vessel at the end of purification process

Measurements of interest elements were performed using a quadrupole mass spectrometer without an isobaric interference suppression system like collision cell. A semiquantitative analytical method was adopted since large numbers of elements must be screened to manage purification plant. Tuning solution at $10*10^{-9}$ g/g Li, Y, Ce, Tl was used to calibrate instrument, measurements were performed in semi-quantitative mode.

Results shown in table 3 refer to elements concentration performed by ICP-MS and HR ICP-MS, values are related to each step of purification process.

Table 3 Contaminations in the samples, the concentration values refer to solid samples, the uncertainty is about 30% of given values

	Ge batch 1B.1	**$GeCl_4$ batch 1B.2**	**$GeCl_4$ batch 1B.3**	**GeO_2 batch 1B.10**	**Ge batch 1B.X**	**Index of reduction**
	[10^{-9}g/g]	**[10^{-9}g/g]**	**[10^{-9}g/g]**	**[10^{-9}g/g]**	**[10^{-9}g/g]**	**%**
Element						
Li	85	<5	<5	<5	1400	<94
Be	<20	<5	<5	<5	<20	<75
B	<50	<50	<50	<20	<20	<60
Na	<500	<500	<500	<500	$14*10^3$	no eff.
Mg	$13*10^3$	8200	5400	1000	$39*10^3$	92
Al (HR)	<2000	<1000	<1000	<1000	$24*10^3$	<50
K (HR)	<2000	<2000	<2000	<1000	$13*10^3$	<50
Sc	<200	<200	<200	<100	120	<50
V	160	<100	<100	<5	6300	<97
Cr	15000	2000	<100	<50	$14*10^5$	<99
Mn	2700	120	<20	<20	<20	<99
Fe (MR)	$62*10^4$	<1000	<1000	<1000	$52*10^5$	<99
Co	140	<10	<5	<5	$96*10^3$	<96
Ni	$11*10^3$	470	<20	<20	$12*10^6$	<99
Cu	$15*10^3$	440	<100	<100	$76*10^5$	<99
Zn	<100	<100	<100	<100	1300	no eff.
Ga	6500	2200	<50	<5	6400	99
As (HR)	<1000	<1000	<1000	<1000	$20*10^3$	no eff.
Rb	<20	<10	<10	<5	<50	<75
^{88}Sr	<20	<20	<10	<10	7600	<50
Mo	4500	1200	<50	<20	$92*10^5$	<99
Ag	1400	100	<20	<20	$89*10^4$	<99
Cd	<50	<20	<20	<20	1300	<60
Sb	140	<10	<10	<10	1400	<93
Cs	<200	<200	<200	<200	<200	no eff.

Ba	50	<15	<15	<10	$83*10^3$	<80
La	<5	<5	<5	<5	120	no eff.
Ce	<5	<5	<5	<5	1000	no eff.
Pr	<5	<5	<5	<5	100	no eff.
Sm	<10	<10	<10	<10	<400	no eff.
Eu	<5	<5	<5	<5	<50	no eff.
Tb	<5	<5	<5	<5	<20	no eff.
Dy	<5	<5	<5	<5	<10	no eff.
Ho	<5	<5	<5	<5	<10	no eff.
Er	<10	<10	<10	<10	<20	no eff.
Tm	<5	<5	<5	<5	<20	no eff.
Yb	<5	<5	<5	<5	<20	no eff.
Lu	<5	<5	<5	<5	<50	no eff.
Hf	<5	<5	<5	<5	<100	no eff.
W	<200	<200	<200	<200	$33*10^4$	no eff.
Os	<10	<10	<10	<10	$19*10^3$	no eff.
Pt	$38*10^3$	660	<20	<10	$42*10^7$	<99
Au	<100	<100	<100	<20	$44*10^3$	<80
Hg	<20	<20	<20	<20	690	no eff.
Tl	<30	<30	<30	<30	180	no eff.
Pb	7500	750	90	<20	10^5	<99
Bi	<20	<20	<20	<20	190	no eff.
Th	<2	<2	<2	<2	85	no eff.
U	<2	<2	<2	<2	140	no eff.

Based on data shown in Table 1, it's possible to declare that first reaction in reactor can be considered total, in fact starting from 500 g of ^{76}Ge kerf only 1 g of waste product is obtained; for this reason, purification process efficiency was very high. From analysis of Table 2, it's possible to see especially for lighter elements that their concentration is significantly reduced during chlorination step, then distillation almost completely separates impurities in starting material. A fundamental aspect to take into consideration is that

distillation can be monitored in real time to evaluate performance and efficiency, suitable to decide when it can be stopped.

As shown in table 4, measure of Al, K, Mn, Fe, are affected by interferences of some chemical adducts from elements usually present in torch, as Ar, O, N; with use of high resolution, it becomes possible to partially resolve these interferences; calculated resolution values to solve isobaric interferences. Three different resolutions are possible with Element 2 spectrometer: low (R=300), medium (R=4000), high (R=10000).

Table 4 Possible interferences observed during acquisition

Element	Isotope (Amu)	Abundance	Interferences	Mass Resolution [1]
	(amu)	(%)		
Al	27	100	$^{11}B^{16}O$, $^{12}C^{15}N$	1450
K	39	93.26	$^{38}Ar^{1}H$	5540
Cr	52	83.79	$^{12}C^{40}Ar$	2375
Fe	56	91.75	$^{40}Ar^{16}O$	2500
As	75	100	$^{40}Ar^{35}Cl$, ^{76}Ge tail	7770
Mo	95	15.84	$^{76}Ge^{19}F$	6800
Cd	111	12.80	$^{76}Ge^{35}Cl$	7960

An important issue regards to high concentration of metals kept in vessel after purification process, chlorination is not selective for those elements; so high amount of impurities doesn't circulate inside plant, thus avoiding dirtying it.

4.1.4.3 Isotope analysis

Purpose of this measure is to determine non-variation of isotope enrichment during purification process, through monitor analysis on starting material and final product.

High importance is related to isotopic enrichment, as cost of enriched germanium significantly varies as percentage of enrichment increasing; after several characterization carried out on several production batch before and after purification, it was possible to

declare non-variation of isotopic enrichment. This procedure has been applied on both type of sample, metal Ge and GeO_2. Results of isotopic characterization are shown in Table 5.

Table 5 Isotopic composition measured in the samples applying mass bias correction

	^{70}Ge/Tot	**^{72}Ge/Tot**	**^{73}Ge/Tot**	**^{74}Ge/Tot**	**^{76}Ge/Tot**
	[%]	**[%]**	**[%]**	**[%]**	**[%]**
Ge kerf sample 1	0.0006 ± 0.0002	0.0010 ± 0.0002	0.011 ± 0.02	7.1 ± 0.5	92.9 ± 1.0
GeO_2 end cycle	0.0005 ± 0.0001	0.0009 ± 0.0002	0.010 ± 0.02	7.0 ± 0.4	93.1 ± 1.1

A correction factor applied during isotopically analysis is mass bias correction, based on different % each Ge isotope. ICP-MS technique is more sensitive to high mass, in this case higher mass is also Ge isotope with higher % of enrichment; with mass bias correction is possible to apply a correction especially for lower isotopes, using a standard germanium solution of natural isotopic composition.

4.2 Copper

Copper is widely used in nuclear physics experiments for different purposes, i.e., detectors assembly and cryostats shielding due to its thermal conductivity capability. It's common to find copper components in rare event physics, such as experimental searches for dark matter[166–171], neutrino physics[172,173] and rare nuclear[174,175].

A common choice for copper use is related to low presence of long-lived Cu radioisotopes with half-life of 61.8 hours[176], ^{67}Cu is longest-lived. Isotopes cosmogenically induced in copper to take under consideration in physical application are ^{56}Co, ^{57}Co, ^{58}Co, ^{60}Co, ^{65}Zn, ^{59}Fe, ^{54}Mn, ^{46}Sc[177].

4.2.1 Samples description

Several copper batches were studied in this work, the first is cylindrical called “billet” which can feature diameters of 89-500 mm, the second one is a cuboid called “cake”, which may have a cross-sectional area featuring width of 405 - 1280 mm and height of 140 – 335 mm, fig 19. Shape and size are defined by the casting mould called “Kokille” (a carbonaceous compound), fig. 20. The inner surface of the mould is composed by carbonaceous compound. This surface is in contact with copper during casting process, so that contamination of mould could potentially led to an increased impurity on the surface of copper cakes and billets.

a (billet) b (cake)

Fig. 19 Shapes of copper batches

c (mould for billet) d (mould for cake)

Fig. 20 Moulds used in casting process defining shape of Cu billets and cakes

During production of billets and cakes, copper sample undergoes an electroforming process to obtain greater chemical purity and electrical conductivity. Moreover, contamination of Th and U were determined also in cathode used in this treatment in order to evaluate its possible role in contamination regards to electroformed copper.

4.2.2 Experimental section

4.2.2.1 Samples Treatment

Copper samples were rinsed by acid cleaning solution Elma Clean 60 at 40°C for 20 minutes in ultrasonic bath to eliminate surface impurities such as oil from shaping/cutting. A preliminary study was conducted on estimation of Cu mass to dissolve and concentration of etching solution, in order to find best conditions.

Chemicals used in sample preparations were HNO_3 ultra-pure grade obtained from Hyper pure grade nitric acid (VWR Chemicals, Canada) through sub-boiling system (DuoPur, Milestone, Italy), H_2O UP (resistivity 18.2 MΩ/cm at 25°C) obtained from a Milli-Q (Millipore Corporation, Billerica, Ma, USA). All measurements were performed by mean Sector Field High Resolution Inductively Coupled Plasma-Mass Spectrometer (Element II, Thermo Fisher Scientific, USA) equipped with an ASX520 autosampler from Cetac (Omaha, NE, USA).

Matrix separation was carried out through TRU columns (Triskem, France) to determine Th and U content. TRU resins characteristics and properties are given by the synergistic combination of CMPO (octylphenyl-N, N-di-isobutyl carboamyle phosphine oxide) extractant diluted in TBP (tributyl phosphate).

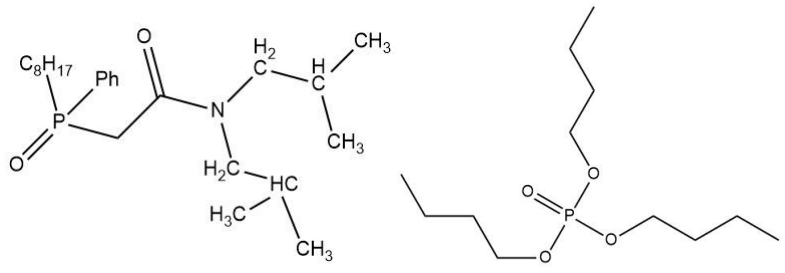

CMPO TBP

Columns have been conditioned by alternate rinsing steps using 5 ml nitric acid 4M and 5 ml of $(NH_4)_2C_2O_4$ (ammonium oxalate) 0.1M (Carlo Erba Reagents, Italy). Several ammonium oxalate commercial solutions were tested from different sellers, in order to evaluate Th and U content in each solution; measurements were performed before and after elution in chromatography columns, obtained values are compared also to estimate efficiency of resins. Washing cycles have been checked continuously until reach low background refers to Th and U, the subsequent elution was carried out with 10 ml of $(NH_4)_2C_2O_4$.

Blank procedure was prepared by mixture with 10 ml H_2O UP and 13 ml of HNO_3 UP, it was eluted and measured to check Th and U content in columns, this operation was carried out to assign each etching solution to each column in order to maximize yield of extraction. Blank of columns was measured after 4-5 washing cycle, purpose was to estimate background of columns in order to apply procedure of blank subtraction on copper samples after ICP-MS characterization. For each column, background measured was not negligible ($0.02 – 0.3 * 10^{-12}$g/g); it was possible to admit ammonium oxalate solution have a not irrelevant background. During data analysis blank contribution must be considered in order to quantify Th and U content. Cu dissolved in etching solution has been loaded into columns that have been eluted with 10 ml of ammonium oxalate solution $(NH_4)_2C_2O_4$.

ICP-MS characterizations were carried out in the same conditions previously used. Briefly, for each column its respective blank has been subtracted procedure to determine Th and U content in each sample. Standard solution of 25 ppt Th and U (AccuStandard, New Haven, USA) in oxalate was used as a reference material to calibrate instrument.

Nevertheless, this extraction system is the only one allowed with this type of columns, so background of columns can be reduced by oxalate ammonium solution.

Experimental procedures and analytical measurements were performed inside a clean room ISO 6 at LNGS to reduce risk of possible environmental contamination.

Regards to kokille, an aliquot of fine powder of ~ 0.3 g was treated with HNO_3 UP in PFA vial previously cleaned and checked at 120°C for 4 hours. Solution was kept under stirring to

increase dispersion of powder; after sample leaching, dilution factor 300 was carried out in order to perform analysis. ICP-MS analysis was followed already adopted procedure for copper samples using same solution to calibrate instrument, a recovery test was carried out in order to estimate mineralization process.

4.2.2.2 Results

Results of HR ICP-MS measurements carried out on mould surface sample are shown in Table 6. It appears a slight diffusion of atoms from mould to copper during casting process, it could be potentially led to increase contamination levels on surface of copper cakes and billets. Regarding Th and U concentrations in cathode, values are found to have same order of magnitude in agreement with copper samples.

Table 6 ^{232}Th and ^{238}U content measured in "kokille" and cathode. Concentrations are blank subtracted and refer to solid sample

Sample	**Th (10^{-9}g*g^{-1})**	**U (10^{-9}g*g^{-1})**
Surface of "Kokille" (mold)	140 ± 40	60 ± 20
	Th (10^{-12}g*g^{-1})	U (10^{-12}g*g^{-1})
Bulk of "cathode"	0.9 ± 0.3	0.6 ± 0.2

After a preliminary evaluation of copper amount to dissolve, in Table 7 mass of initial copper samples "K" and "L" as well as dissolved mass in consecutive etching steps are shown. The measured contamination levels are described in Table 8, removed material in first etching step features rather large amount of impurities (though still three orders of magnitude lower than in the mold), while in the following etching steps the concentrations of ^{232}Th and ^{238}U quickly decreases. By conversion of dissolved mass in each etching step to removed surface thickness, it was possible to plot a contamination depth profile for both samples, as shown fig. 21.

Many recovery tests were carried out to quantify the efficiency extraction of columns and recovery values obtained for Th and U were always > 90%. These results confirm procedure used for matrix extraction of Th and U was suitable; regarding detection limits, values of $0.4*10^{-12}$ g/g were reached.

Table 7 Etching of Cu samples, table documents amount of Cu dissolved and measured in each etching step

Etching	**Sample "K"**			**Sample "L"**		
	Weight (g)	**Dissolved (g)**	**Comment**	**Weight (g)**	**Dissolved (g)**	**Comment**
Starting material	23.28			25.3		
step 1	20.2	3.08	mesasured	22.02	3.28	mesasured
step 2	17.07	3.13	mesasured	18.79	3.23	mesasured
step 3	13.72	3.35	mesasured	15.47	3.32	mesasured
step 4	10.41	3.31	mesasured	12.21	3.26	mesasured
step 5	7.59	2.82	mesasured	9.02	3.19	mesasured
step 6	4.43	3.16	mesasured	5.9	3.12	mesasured
step 7	1.37	3.06	mesasured	3.29	2.61	mesasured
step 8	0.01	1.36	spiked 25 ppt	0.15	3.14	spiked 25 ppt

Table 8 Contamination in Cu samples, concentration values refer to solid sample; uncertainty is about 30% of given values

Etching	Sample "K"			Sample "L"		
	Depth (mm)	Th (10^{-12}g/g)	U (10^{-12}g/g)	Depth (mm)	Th (10^{-12}g/g)	U (10^{-12}g/g)
step 1	0.00 – 0.30	250 ± 80	250 ± 80	0.00 – 0.30	75 ± 22	112 ± 33
step 2	0.30 – 0.64	25 ± 7	10 ± 3	0.30 – 0.63	10 ± 3	5 ± 1.6
step 3	0.64 – 1.05	14 ± 4	2.4 ± 0.7	0.63 – 1.01	7 ± 2	4 ± 1
step 4	1.05 – 1.53	10 ± 3	1.6 ± 0.5	1.01 – 1.44	5 ± 2	3 ± 1
step 5	1.53 – 2.03	7 ± 2	1.3 ± 0.4	1.44 – 1.94	3 ± 1	1.5 ± 0.4
step 6	2.03 – 2.76	6 ± 2	0.7 ± 0.2	1.94 – 2.55	1.3 ± 0.4	0.8 ± 0.2
step 7	2.76 – 3.94	4 ± 1	0.6 ± 0.2	2.55 – 3.26	n.a.	n.a.
step 8	3.94 – 5.46	n.a.	n.a.	3.26 – 5.16	n.a.	n.a.

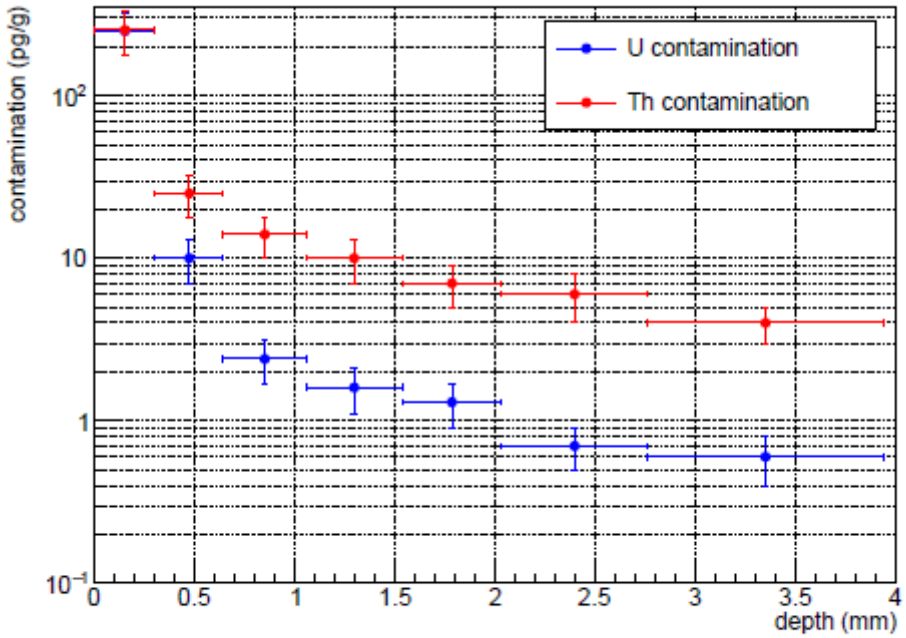

(a) "K".

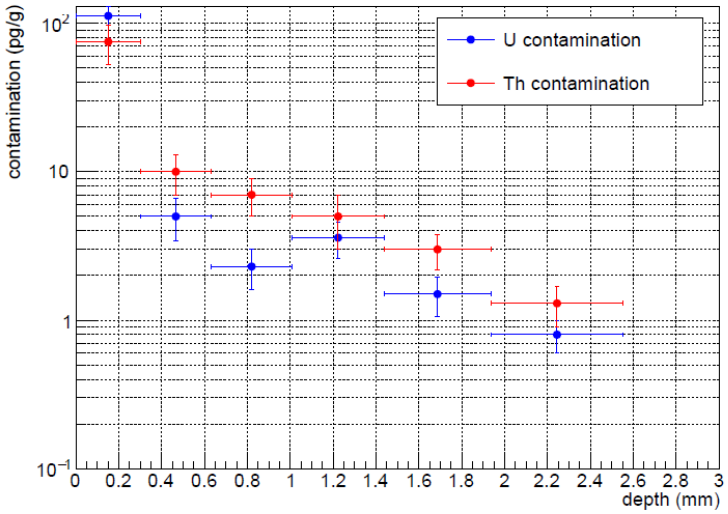

(b) "L".

Fig. 21 Depth profile of ^{232}Th and ^{238}U contamination in samples "K" and "L"; depth uncertainity takes into account thickness of material removed from surface in every single step. Uncertainities on contaminant represent measurement uncertainties of about 30%

4.3 Electronic devices

Nowadays there's a notable increase in printing technologies applied to various applications, also in scientific research; electronic devices with increasing performance, wide adaptability, high storage capability, etc, are manufactured daily both at industrial level and small laboratory production level.

4.3.1 Samples description

During setup of astroparticle physics experiments, different types of circuits are studied and subsequently used to find best electronic devices; this step is very important to setup an efficient system directly connected to detectors for acquire, record and store signals received from experiments.

In widely variety of circuits so far designed and developed in electronic industry, Print Circuit Board (PCB) finds widespread use in scientific research, i.e., astroparticle physics experiments. PCB is a multilayer structure that supports components and interconnects

them by copper wiring. PCB is composed of copper and woven composite layers as a core, sometimes additional copper layers are linked to core by prepreg layers; woven composite is an epoxy and glass fiber composited and polymerized prepreg are general assumed to exhibit similar thermomechanical properties[178]. Also silicon photo multiplier (SiPM) are widely used in physics experiments following same behaviour of PCB.

4.3.1 Experimental section

4.3.2.1 Samples treatment

Given complex conformation of PCB due to presence of multilayers, their characterization provides a preliminary approach to decide sample's treatment. Silicon is predominant element in PCB, like most electronic components used in several applications; furthermore, gold, iron, aluminum, are need on upper layer of circuits as additional support in order to solder inductors, sensors, etc.

First characterization is related to separation of contribution refers to metal part and glass part. Mineralization by acid solutions is the only way to perform ICP-MS analysis, acid etching is need to solubilize metal tracks printed on support, thermal heating is required to speed up and maximize solubilization; operative conditions could be described as use of PFA vial in order to reach high temperatures (150°C – 180°C), ultra-pure water (resistivity 18.2 MΩ/cm at 25°C) was obtained from a Milli-Q (Millipore Corporation, Billerica, Ma, USA), ultra-pure grade nitric acid was obtained from Hyper pure grade nitric acid (VWR Chemicals, Canada) using a sub-boiling distillation system (Milestone, Sorisole, BG, Italy) and ultra-pure hydrofluoric acid were also used to perform solubilization.

A low amount of circuit was dissolved in HCl at high T to solubilize metal slopes, only track have been etched by HCl due to presence of gold; obtained solution was picked up using a pipette and retained in clean vial, ultrapure water was added to perform dilution for ICP-MS characterization. Silicon mainly was rest part of circuit, a mixture HF/HNO_3 in ratio 3/1 was used to mineralize Si at high T, HF addition in different times became necessary to

solubilize whole sample. Several tests were performed in order to find best ratio circuit/acid, it has been observed best relationship in ratio 1/5. After total dissolution of Si, a further T increase was carried out to perform HF evaporation; just only HNO_3 was left in vial, ultrapure water was added to recover sample at 80°C.

Spike solution was carried out to perform recovery test, standard addition has been performed after etching by HCl to avoid loss of solution during transfer. Idea of separating radioactive contribution of metallic and glass components considering them as two different samples, has allowed to have a more detailed knowledge of characterized sample.

4.3.2.2 Analysis and results

Solutions were diluted up to DF 2000-4000 to perform ICP-MS analysis; quantitative analysis was carried out with in order to determine amount of K, Pb, Th U in samples.

Instrumental sensitivity was monitored before analysis using tuning solution at $1*10^{-12}$g/g by Thermo Fisher Scientific, calibration was performed with standard solution of interest elements (K, Pb, Th, U). It was also possible also to distinguish radioactive contribute coming from metals than contribute from silicon, due to two separate mineralization of PCB. Highest contribution was relative to lead and potassium in metal part, so it was possible to state contamination mainly comes from slopes and their welding process, results shows in Table 8.

Table 8 Contaminations in SiPM, concentration values refer to solid sample; values uncertainty is ~ 30%, recovery of Th and U were 99%, about K 98%

Silicon Photo Multiplier					
Part	**Unit**	**Th (LR)**	**U (LR)**	**K (HR)**	**Pb (LR)**
Metals	10^{-9} g/g	0.95 ± 0.29	1.1 ± 0.3	1700 ± 510	7000 ± 2100
Silicon	10^{-9} g/g	< 0.5	< 0.1	< 2000	< 200

4.4 Metals

Use of metals is central to advance of technology, through various properties as conductivity, ductility, high T_m. They can also be processed by several means (i.e., alloying, cold working, heat treating) to give them high strength or other desirable properties by producing imperfections in regular repeat patter of crystalline structure within metals[179]. Metal compounds fine wide applications in underground infrastructure as support of detectors, shielding, conductors, etc…

Radiopurity of these of materials is largely important, as various applications to which it can be subjected require different levels of contamination; unlike copper, other metal as steel, aluminum, iron must be treated following a different type of etching to allow their solubilization.

4.4.1 Treatment

Steel samples were rinsed with cleaning solution Elma Clean 60 at 40°C for 20 minutes in ultrasonic bath to superficial impurities coming from machine work.

Regarding steel and iron samples, first step concerned search for a solvent or a mixture able to solubilize metals; differently from copper, it was observed that even high concentration HNO_3 had no effects on samples dissolution. To perform solubilization of steel samples, mixture of HCl/HNO_3 in ratio 5/1 was turned out to be best solution.

Etching was performed in PFA vial by solution 10 ml HCl and 2 ml HNO_3, with this amount of solvent about 2 g of steel was removed by each etching; obtained solution were collected separately in PFA vials cleaned and checked before use, shown Table 9. All solution were diluted before ICP-MS characterization to reach DF in range 3000-5000.

Table 9 Description of steel samples

Sample 1	Weight (g)	Steel dissolved (g)	Note
Starting material	34.59		
Etching n. 1	33.32	1.29	Waste
Etching n. 2	31.54	1.76	Waste
Etching n. 3	29.61	1.93	Measured
Etching n. 4	28.03	1.58	Measured
Sample 2	**Weight (g)**	**Steel dissolved (g)**	**Note**
Starting material	33.33		
Etching n. 1	32.08	1.25	Waste
Etching n. 2	30.41	1.67	Waste
Etching n. 3	28.28	2.13	Measured
Etching n. 4	26.61	1.68	Measured
Sample 3	**Weight (g)**	**Steel dissolved (g)**	**Note**
Starting material	10.94		
Etching n. 1	9.64	1.3	Waste
Etching n. 2	8.15	1.49	Waste
Etching n. 3	6.76	1.39	Measured
Etching n. 4	4.99	1.77	Measured
Sample 4	**Weight (g)**	**Steel dissolved (g)**	**Note**
Starting material	15.24		
Etching n. 1	14.11	1.14	Waste
Etching n. 2	12.18	1.92	Waste
Etching n. 3	10.46	1.72	Measured
Etching n. 4	8.97	1.49	Measured

Sample 5	Weight (g)	Steel dissolved (g)	Note
Starting material	14.61		
Etching n. 1	13.41	1.2	Waste
Etching n. 2	11.64	1.77	Waste
Etching n. 3	9.93	1.71	Measured
Etching n. 4	8.47	1.46	Measured

Sample 6	Weight (g)	Steel dissolved (g)	Note
Starting material	14.42		
Etching n. 1	13.14	1.28	Waste
Etching n. 2	11.68	1.46	Waste
Etching n. 3	9.94	1.74	Measured
Etching n. 4	8.49	1.45	Measured

Sample 7	Weight (g)	Steel dissolved (g)	Note
Starting material	4.25		
Etching n. 1	3.81	0.44	Waste
Etching n. 2	3.02	0.81	Waste
Etching n. 3	2.31	0.69	Measured
Etching n. 4	1.73	0.58	Measured

Sample 8	Weight (g)	Steel dissolved (g)	Note
Starting material	5.98		
Etching n. 1	5.31	0.68	Waste
Etching n. 2	4.52	0.78	Waste
Etching n. 3	3.71	0.82	Measured
Etching n. 4	2.95	0.75	Measured

Sample 9	**Weight (g)**	**Steel dissolved (g)**	**Note**
Starting material	6.16		
Etching n. 1	5.65	0.51	Waste
Etching n. 2	4.49	1.16	Waste
Etching n. 3	3.79	0.7	Measured
Etching n. 4	3.32	0.47	Measured

4.4.2 Analysis and results

Characterization was performed by HR ICP-MS to determine amounts of Th and U in 9 steel samples from 3 different production batches, sampling in different sites on steel billets; purpose of this characterization was to select best production batch in order to planning subsequent activities.

In Table 10 are shown results of ICP-MS characterizations, etching 3 and etching 4 were considered in this study because referring to bulk. Surface contamination should not have been significant due to thickness removed from previous etching.

Spike solution was carried out to evaluate recovery of Th and U, a known amount of standard solution was added to one sample before etching and resulted recovery was in order of 99% for Th and U; moreover, calibration was performed by reference standard solution of $100*10^{-12}$ g/g Th and U (AccuStandard, New Haven, USA).

Table 10 Contamination in steel samples, concentration values refer to solid sample; uncertainty is ~ 30% of given values, recovery of Th and U were in the order of 99%

Contamination in steel samples 1 2 6					
	Details	**Unit**	**Sample 1**	**Sample 2**	**Sample 6**
^{232}Th (MR)	**Etching 3**	10^{-12} g/g	951 ± 285	380 ± 114	1065 ± 320
^{238}U (MR)	**Etching 3**	10^{-12} g/g	5470 ± 1640	3432 ± 1030	4405 ± 1322
^{232}Th (MR)	**Etching 4**	10^{-12} g/g	1250 ± 375	328 ± 98	1423 ± 427
^{238}U (MR)	**Etching 4**	10^{-12} g/g	7501 ± 2250	4678 ± 1403	5592 ± 1678
Contamination in steel samples 3 4 5					
	Details	**Unit**	**Sample 3**	**Sample 4**	**Sample 5**
^{232}Th (MR)	**Etching 3**	10^{-12} g/g	74 ± 22	762 ± 229	1618 ± 485
^{238}U (MR)	**Etching 3**	10^{-12} g/g	128 ± 38	3790 ± 1137	7403 ± 2221
^{232}Th (MR)	**Etching 4**	10^{-12} g/g	61 ± 18	753 ± 226	2063 ± 619
^{238}U (MR)	**Etching 4**	10^{-12} g/g	59 ± 18	5408 ± 1622	9714 ± 2914
Contamination in steel samples 7 8 9					
	Details	**Unit**	**Sample 7**	**Sample 8**	**Sample 9**
^{232}Th (MR)	**Etching 3**	10^{-12} g/g	1090 ± 327	273 ± 82	567 ± 170
^{238}U (MR)	**Etching 3**	10^{-12} g/g	365 ± 110	< 100	95 ± 29
^{232}Th (MR)	**Etching 4**	10^{-12} g/g	434 ± 130	67 ± 20	610 ± 183
^{238}U (MR)	**Etching 4**	10^{-12} g/g	106 ± 32	13 ± 4	211 ± 63

4.5 Plastics

Applications of plastic materials are very used in physics experiments due to their high radiopurity and adaptability, components are present in every system makes up an

experimental apparatus; therefore, currently these materials are screened to monitor their radiopurity. In our field of research, plastic material is widely used in electronic devices, shielding, support, containment, coverage.

Given wide variety of plastic types, sample mineralization to perform ICP-MS characterization depends on each type of plastic; ashing treatment and recovery by acid could be procedures to mineralize samples, but also other solution can be performed i.e., microwave digestion.

4.5.1 Treatment

First step to carry out to characterize plastic samples was mineralization of sample, ashing procedure was performed by use of muffle, subsequently recover by acid solution was carried out in order to obtain a ready solution for ICP-MS.

During cutting of samples, an amount of 3 g was weighed after initial evaluation of ideal mass to treat; rinsing was carried out by acid cleaning solution in ultrasonic bath at 40°C for 20 min, in order to remove grease, oil and other similar compounds coming from handling. Subsequently, samples were placed into crucibles to perform ashing at 650°C for 4 hours using a muffle apparatus, fig. 22.

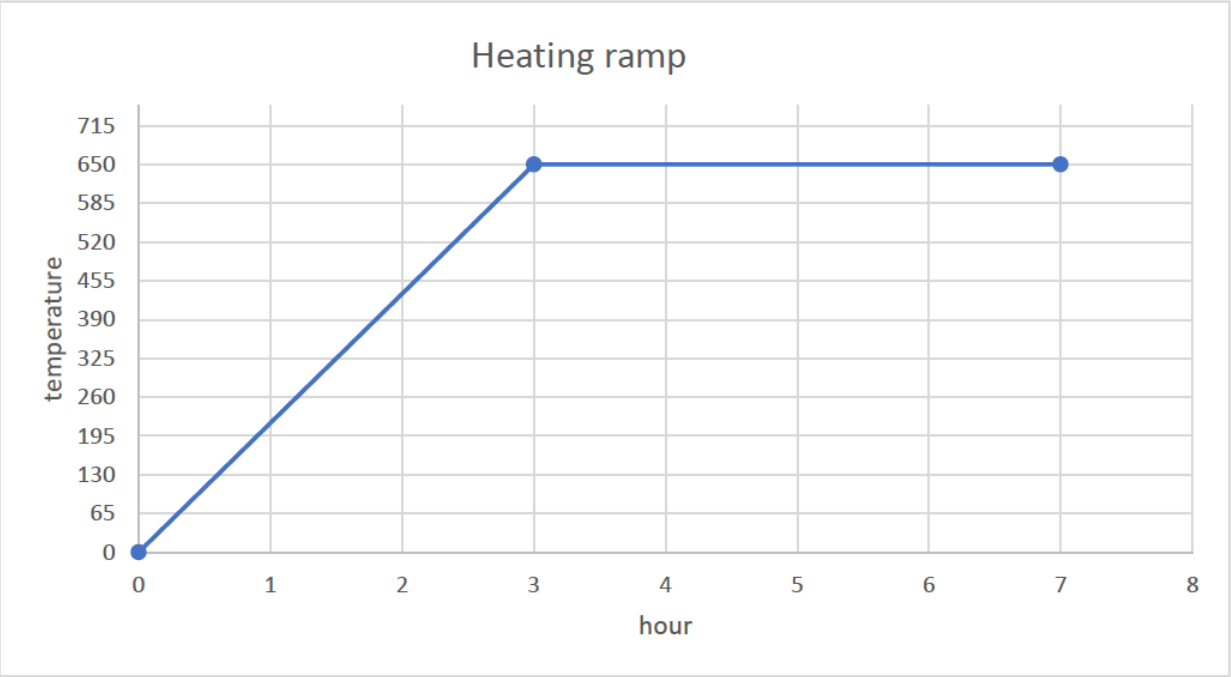

Fig. 22 Heating ramp of muffle

After ashing procedure, crucibles have been filled with HNO_3 10% solution and they're placed in oven at 80°C for recovery procedure of samples. Obtained solution with were pipetted into clean vials to carried out ICP-MS analysis.

Focusing on crucibles, quartz crucibles and platinum crucibles are used depending on type of sample to be characterized; this feature is very important in order to measure ultra-trace and to reach low detection limit, also quality of crucible's material is important to know at the beginning.

In case of polytetrafluoroethylene (PTFE), quartz crucibles cannot use to avoid them degradation. PTFE is fluorinated compound, as it's a high-molecular weight polymer consisting wholly of carbon and fluorine; during ashing process, reaction of PTFE with air generates HF which is able to etch quartz and thus degrade it. A possible solution to avoid this nasty inconvenience is through use of platinum crucibles, taking care to check their contamination (blank of crucibles). Anyway, PTFE is widely used in physics experiments because its purity is naturally high compared to other plastic materials.

With regards on other types of plastics, as polyethylene, nylon, ultem, peek, torlon, etc…, quartz crucibles are an excellent container for ashing thanks to its resistance to high T reached necessary for this treatment.

4.5.2 Analysis and results

ICP-MS characterization was performed to measure content of ^{39}K, ^{232}Th, ^{238}U in wide variety of samples. Regards to potassium quantification, high resolution mass spectrometer was always used to perform analysis, shown in Table 11 and Table 12. During mineralization, spike solution of known amount of K, Th, U was added at the end of process; high recovery % (>95%) were reached for Th and U in many samples, regards K low recovery values (50%-60%) were determined due to difficult of quantification by ICP-MS due to interference of $^{38}Ar^{1}H$.

Several screening campaigns were conducted on plastic samples, it was possible to declare best material for each specific use, also discrimination about each single production batch was possible to conduct through ICP-MS results. Some chemical compound can be applied on surface of plastic materials to expand their application, i.e., wavelength shifter (tetraphenyl-butadiene, parylene), α-particle shielding; also characterization of organic compounds were carried out in order to evaluate radioactive contribute coming from process of coating, a comparison between "pure" and covered material was carried by measurement.

Table 11 Contaminations measured in PTFE samples, values refer to solid sample

PTFE samples							
Element	**Unit**	**Powder 1**	**Powder 2**	**Powder 3**	**Powder 4**	**Powder 5**	**Slab**
^{232}Th (LR)	10^{-12} g/g	1.7 ± 0.5	1.1 ± 0.3	74.5 ± 22.4	18.2 ± 5.5	3.3 ± 1.0	5.3 ± 1.6
^{238}U (LR)	10^{-12} g/g	4.0 ± 1.2	11.1 ± 3.3	13.5 ± 4.1	200.3 ± 60.1	0.5 ± 0.2	4.4 ± 1.3
		Powder 6	**Powder 7**	**Powder 8**	**Powder 9**	**Powder 10**	
^{232}Th (LR)	10^{-12} g/g	0.9 ± 0.3	< 2	7.8 ± 2.3	< 2	3.8 ± 1.1	
^{238}U (LR)	10^{-12} g/g	30.2 ± 9.1	15.9 ± 4.8	144.0 ± 43.2	< 2	204.1 ± 61.2	

Table 12 Contaminations measured in plastic samples, values refer to solid sample

Some particular plastic sample and their derivants								
Element	**Unit**	**Pellet**	**Polistyrene**	**Vikuiti**	**PE borate**	**Parylene**	**PEN**	**Solder glue**
^{232}Th (LR)	10^{-12} g/g	< 10	< 5	< 2	1.3 ± 0.4	38.7 ± 11.6	88.6 ± 26.4	2.9 ± 0.8
^{238}U (LR)	10^{-12} g/g	< 10	< 5	1.8 ± 0.6	2.1 ± 0.6	17.5 ± 5.3	75.3 ± 22.5	64.4 ± 19.4
^{39}K (HR)	10^{-12} g/g		< 50			71.8 ± 21.6	1000 ± 400	11.2 ± 3.4

Recovery test was carried out using standard solution of $100*10^{-12}$ g/g Th and U and $100*10^{9}$ g/g K (AccuStandard, New Haven, USA), calibration and instrumental sensitivity was checked by standard reference solution.

4.6 Radio-biological measurements

To further characterize the radioactive background of biological experiments, intrinsic contribution of radioactivity in this experimental set (plugs, vials and culture medium) was carried out by gamma-ray spectrometry with high pure germanium (HPGe) detectors and Inductively Coupled Plasma Mass Spectrometry (ICP-MS).

The analysis was carried out by these two different techniques taking advantage of the LNGS expertise for the measurement of low-level radioactivity applied to the study of rare fundamental physics phenomena, such as double-beta decay, nuclear decays and dark matter [149,180]. However, both HPGe spectrometry and ICP-MS are analytical techniques that are also commonly used for trace element determination in other fields. For what is concerning the natural decay chains of uranium and thorium, HPGe spectrometry and ICP-MS address different nuclides. They also have different sensitivity and times of measurement, ICP-MS being usually much faster and more sensitive to uranium and thorium themselves, whereas gamma-ray spectrometry is more sensitive to the gamma-active shorter-lived progenies within their decay chains, but with longer measurements times. A

combination of both can usually give a complete picture on the status of the decay chain and can identify possible ruptures of the secular equilibrium within it. Furthermore, ICP-MS is considered a destructive technique that requires elaborate sample processing prior the analysis. On the other hand, HPGe spectrometry allows for very easy sample handling although it requires long time of measurement and a large amount of sample. Usually, the choice of one over the other technique depends on the physical properties related to sample, the amount of available sample and time. It is important to point out that ICP-MS analysis directly quantifies the concentration of ^{39}K and the concentration/specific activity of ^{40}K is derived based on its natural isotope abundance (0.012%).

Each experimental set consists of a polypropylene vial weighing about 6.6 grams, a cellulose acetate plug weighing about 1.5 grams and Nutrifly medium weighing about 7 grams, fig. 23.

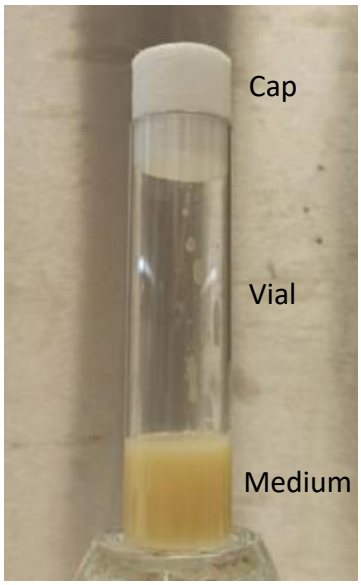

Fig. 23 Experimental set of RENOIR experiment

As expected, the major contribution in term of specific activity comes from ^{40}K. The results from the two analyses are in good agreement with each other, especially for the ^{40}K activity, Table 13.

4.6.1 Experimental section

4.6.1.1 Sample treatment

Microwave assisted digestion was carried out to perform analysis of food flies, this choice was made as it proved to be very effective for complete mineralization of samples; an amount of 500 mg was used to process digestion, specific method has been fine-tuned to this procedure. Ramp start for 15 min at 1800 W to reach 200°C, which have been kept constant for other 15 min, then they gradually decrease to perform cooling down. Procedure made use of HNO_3 UP and H_2O_2 30% in ratio 4/1 up to 25 ml with an amount of sample about 500 mg.

Regarding mineralization of vials and plugs, 3 g and 1.5 g respectively were incinerated in muffle at 650°C for 4 hours, crucibles used were previously rinsed with 10 ml of 10% UP HNO_3 and they have been measured before each treatment. One portion of each sample was used to estimated K, Th, U, recovery efficiency adding a known amount of reference solution (Th U $100*10^{-12}$ g/g, K $1000*10^{-9}$ g/g).

Drosophila flies were treated in hotplate to obtain complete solubilization, during first cycle 1 ml of HNO_3 UP and 0.1 ml of H_2O_2 30% were used at 120°C for 1 hour, then 8 ml of H_2O UP was added to dissolve total amount of sample; subsequently 1 ml of HNO_3 UP and 4 ml of H_2O UP were used in two different moments to washing vials and to recover sample's trace still inside vials.

4.6.1.2 Reagents

Chemicals used in samples preparation were HNO_3 ultra-pure grade (VWR Chemicals, Canada), it obtained through sub-boiling system (DuoPur, Milestone, Italy), H_2O ultra-pure (resistivity 18.2 MΩ/cm at 25°C) obtained from a Milli-Q apparatus (Millipore Corporation, Billerica, MA, USA). A closed-vessel microwave system (Ethos UP, Milestone, Sorisole, Italy) equipped with fiber-optic temperature sensor was used for performing digestions, instrument was equipped with a rotor with 6 PTFE vials with volume of 100 ml. All

measurements were performed by mean Sector Field High Resolution Inductively Plasma Mass Spectrometer (Element II, Thermo Fisher Scientific, USA) with an ASX520 autosampler from Cetac (Omaha, NE, USA).

4.6.1.3 Results and discussion

Characterization carried out with ICP-MS to estimate ^{40}K, ^{232}Th, ^{238}U content in experimental set: vial, acetate cup, Nutrifly medium dry and mixture were analysed to check contaminants, Table 13. Major contribution in terms of contamination comes from ^{40}K, instead negligible values were measured for Th and U in comparison, exactly as expected since food has a huge amount of potassium and flies naturally have high concentration of potassium as humans, in addition to potassium assimilated directly from their food. Recovery test was also in accordance with sample non spiked, so it's possible to declare different treatments followed to this complex system were effective.

Table 13 Results of experimental setup, values refer to solid sample

Contamination						
Element	**Unit**	**Vial**	**Plug**	**Food dry**	**Mixture**	**Flies**
^{232}Th (LR)	10^{-12} g/g	38.8 ± 11.6	272.1 ± 81.6	5400 ± 1600	700 ± 200	< 200
^{238}U (LR)	10^{-12} g/g	69.3 ± 20.8	197.4 ± 59.2	2700 ± 800	500 ± 200	< 200
^{39}K (HR)	10^{-9} g/g	1360 ± 408	1015 ± 305	$4*10^6 \pm 1*10^5$	$6*10^5 \pm 0.2*10^3$	$3*10^6 \pm 9*10^5$

In addition, gamma-ray spectrometry was adopted to further characterization, to make a comparison and to have a general overview of this experimental setup, Table 14; obtained values are in good agreement with each other especially for ^{40}K activity.

Table 14 Results from ICP-MS and HPGe spectrometry, all values are shown in terms of activity

Specific activity (mBq/kg)							
	ICP-MS				HPGe		
	Vial	Plug	Food	Fly	Vial	Plug	Food
^{232}Th	0.2	1.1	2.8	0.8			
^{228}Ra							< 23
^{228}Th							< 15
^{238}U	0.9	2.4	6.2	2.5			
^{226}Ra					5	< 5.8	< 8.6
^{234}Th					< 340	< 57	< 210
^{234m}Pa					< 220	< 250	< 560
^{40}K	42	32	19*103	93*103	< 45	< 120	17.8*103
^{235}U					< 4.7	< 8	< 19
^{137}Cs					<1.5	< 5.9	< 7
^{7}Be					30		

5 Conclusions and Outlook

The main topic of this thesis is material screening applied to low background experiments, an important approach to establish whether each type of material features sufficient radiopurity to allow its use during the setup of experiments. Regardless of the ultimate goal of each experiment, the screening process is necessary to improve the sensitivity of the experiments.

Development of chemical plant for germanium purification required a strong synergy between chemical characteristics and engineering performance; purpose of this plant was purification of several kilograms of metal germanium through a purification process, a sequence of chemical reactions made it possible to convert dirty metal Ge into purified GeO_2; reduction with H_2 to convert GeO_2 into purified metal Ge, crystal growth and detector's production were sequent steps carried out by other research groups.

Online characterization of starting materials, intermediated products and final products has allowed to follow each reaction involved in all over the process. ICP-MS measurements were optimal way to took decision on roadmap of purification process due to their short analysis time (1-2 h). Concerning needed purification cycles needed to purify several kilograms of Ge, a synchrony with scientists involved in purification process has also made it possible simultaneously purification of two different batch performing cyclically chemical reactions.

Focusing on copper, its use is very wide in several applications and quantification of Th and U content becomes necessary to declare production batch suitable to use for various installations. Studies carried out on pre-concentration and extraction of Th and U made it possible to optimize procedures, several washing cycles of chromatographic columns has allowed to reduce background before extraction of elements. Improving of conditions regards to columns performance were carried out in order to reduce detection limit; several preliminary test on different types of solution, amount of volume, mass of sample ca be evaluated to reach best operative conditions.

Moreover, other materials used in underground experiments are treated and measured by ICP-MS, particularly metals, plastics, glass, organic compounds; dissolution of all samples has required different treatment to follow, large time to find best conditions and maximize quantifications.

About underground biology experiments, total experimental setup was characterized by mass spectrometry measurements, in order to estimate its total intrinsic radioactivity. A parallel study was carried out by gamma-ray spectrometry to have a comparison on contaminations inside samples and to have a general overview of system.

Considering all applications, development of different methods regarding both analytical part and spectrometric part has been fundamental in order to improve performance and materials selection.

Next features can involve development of new system for separation process, in specific case of copper an automatic system regards to continuous purification cycle with no direct interaction by operator; considerable advantages on lowering detection limit could be achieved given reduction of sample handling. Also on chromatographic resins, different stationary phases can be tested to see an eventual reduction of background coming from resins.

Performance on ICP-MS characterizations can be ever maximized through new hardware upgrades and change of instrumental conditions; new spectrometers with different analyzers could be used to have a comparison with different characterizations. Preparation of samples with no dissolution process can be performed to avoid risk of contamination due to handling, especially for materials with initial high purity; laser ablation system could be useful on this way, since given that with this system it’s possible to carry out measurements directly from solid sample.

Starting from several advantages of ICP-MS, it could be possible to extend these types of characterizations to wide variety of matrices, i.e., cultural heritage, as already happened through Cultural Heritage Network of INFN (CHNet); exploration of new fields of application

can increase knowledge of mass spectrometry performance applied to wide variety of materials.

A continuous screening of materials, with aim of trying to further lower detection limit in ICP-MS measurements, it's a first step to arrive at an even more accurate evaluation of radiopurity; use of increasingly pure materials is a fundamental contribution to background reduction. Therefore, there will be an increase in terms of sensitivity for various experiments.

In next future, new experiments will be installed at LNGS with continuous activity of material screening, principal purpose will always try to find material with greater radiopurity in order to achieve high sensitivities.

Bibliography

1. Leonard, D. S. *et al.* Systematic study of trace radioactive impurities in candidate construction materials for EXO-200. *Nucl Instrum Methods Phys Res A* **591**, 490–509 (2008).

2. Arnold, R. *et al.* Performance of a prototype tracking detector for double beta decay measurements. *Nucl Instrum Methods Phys Res A* **354**, 338–351 (1995).

3. Dokania, N. *et al.* Characterization and modeling of a low background HPGe detector. *Nucl Instrum Methods Phys Res A* **745**, 119–127 (2014).

4. Agostini, M. *et al.* Results on Neutrinoless Double-Beta Decay from Phase I of the GERDA Experiment. *Phys Rev Lett* **111**, 122503 (2013).

5. Auger, M. *et al.* Search for Neutrinoless Double-Beta Decay in ^{136}Xe with EXO-200. *Phys Rev Lett* **109**, 032505 (2012).

6. Agostini, M. *et al.* The background in the neutrinoless double beta decay experiment Gerda. *The European Physical Journal C* **74**, 2764 (2014).

7. Bellini, F. *et al.* Monte Carlo evaluation of the external gamma, neutron and muon induced background sources in the CUORE experiment. *Astroparticle Physics* **33**, 169–174 (2010).

8. Andreotti, E. *et al.* Muon-induced backgrounds in the CUORICINO experiment. *Astroparticle Physics* **34**, 18–24 (2010).

9. Argyriades, J. *et al.* Measurement of the background in the NEMO 3 double beta decay experiment. *Nucl Instrum Methods Phys Res A* **606**, 449–465 (2009).

10. Budjáš, D., Heisel, M., Maneschg, W. & Simgen, H. Optimisation of the MC-model of a p-type Ge-spectrometer for the purpose of efficiency determination. *Appl. Rad. and Isot.* **67**, 706–710 (2009).

11. Hardy, J. C. *et al.* Precise efficiency calibration of an HPGe detector: source measurements and Monte Carlo calculations with sub-percent precision. *Appl. Rad. and Isot.* **56**, 65–69 (2002).

12. Helmer, R. G. *et al.* The use of Monte Carlo calculations in the determination of a Ge detector efficiency curve. *Nucl Instrum Methods Phys Res A* **511**, 360–381 (2003).

13. Hernández, F. & El-Daoushy, F. Accounting for incomplete charge collection in Monte Carlo simulations of the efficiency of well-type Ge-detectors. *Nucl Instrum Methods Phys Res A* **498**, 340–351 (2003).

14. Hurtado, S., García-León, M. & García-Tenorio, R. GEANT4 code for simulation of a germanium gamma-ray detector and its application to efficiency calibration. *Nucl Instrum Methods Phys Res A* **518**, 764–774 (2004).

15. Karamanis, D. Efficiency simulation of HPGe and Si(Li) detectors in γ- and X-ray spectroscopy. *Nucl Instrum Methods Phys Res A* **505**, 282–285 (2003).

16. Gomez-Cadenas, J. J. *et al.* Sense and sensitivity of double beta decay experiments. (2010), Jour. of Cosm. and Astrop. Physics, **007**, (2011).

17. Hamajima, Y. & Komura, K. Depth profiles of environmental neutron fluxes in water and lead. *Radio. in the Envir.* **8**, 511–519 (2006).

18. Heusser, G. Low radioactivity Background Techniques. *Ann.l Rev. of Nucl. and Part. Science* **45**, 543–590 (1995).

19. Laubenstein, M. & Lawson, I. Low Background Radiation Detection Techniques and Mitigation of Radioactive Backgrounds. *Front Phys* **8**, (2020).

20. Roszkowski, L., Sessolo, E. M. & Trojanowski, S. WIMP dark matter candidates and searches—current status and future prospects. *Reports on Progress in Physics* **81**, 066201 (2018).

21. Amaré, J. *et al.* Annual modulation results from three-year exposure of ANAIS-112. *Phys. Rev. D* **103**, 102005 (2021).

22. L'Annunziata M. *Hand. of Radio. Anal*. (2012).

23. Tamponnet, C. Behaviour of Lead-210 in continental environment: Comparison with stables isotopes of lead. *Radiopr.* **44**, 285–289 (2009).

24. Pfeiffer, D. Health Physics and Radiological Health, 4th Edition. *Med Phys* **40**, 117301 (2013).

25. Fabian, R., Bell, J. & Brandl, A. A Radon Background-subtraction Algorithm for Electronic Personal Dosimeters. *Health Phys* **119**, 216–221 (2020).

26. Clement, C. H. *et al.* Lung Cancer Risk from Radon and Progeny and Statement on Radon. *Ann ICRP* **40**, 1–64 (2010).

27. Ambrosino, F., Thinová, L., Briestenský, M. & Sabbarese, C. Analysis of radon time series recorded in Slovak and Czech caves for the detection of anomalies due to seismic phenomena. *Radiat Prot Dosimetry* **186**, 428–432 (2019).

28. Negarestani, A., Setayeshi, S., Ghannadi-Maragheh, M. & Akashe, B. Layered neural networks based analysis of radon concentration and environmental parameters in earthquake prediction. *J Environ Radioact* **62**, 225–233 (2002).

29. Planinić, J., Radolić, V. & Lazanin, Ž. Temporal variations of radon in soil related to earthquakes. *Appl. Rad. and Isot.* **55**, 267–272 (2001).

30. Ambrosino, F., Thinová, L., Hýža, M. & Sabbarese, C. ^{214} Bi/ ^{214} Pb radioactivity ratio three-year monitoring in rainwater in Prague. *Nukleonika* **65**, 115–119 (2020).

31. Morishita, Y. *et al.* Optimization of thickness of GAGG scintillator for detecting an alpha particle emitter in a field of high beta and gamma background. *Radiat Meas* **112**, 1–5 (2018).

32. Zeng, C. *et al.* Review of Radon and Its Progeny Measurement Technology in Environmental Gamma Measurement. *J Phys Conf Ser* **1739**, 012024 (2021).

33. Päs, H. & Rodejohann, W. Neutrinoless double beta decay. *New J Phys* **17**, 115010 (2015).

34. Dolinski, M. J., Poon, A. W. P. & Rodejohann, W. Neutrinoless Double-Beta Decay: Status and Prospects. *Ann. Rev. of Nucl. and Part. Science* **69**, 219–251 (2019).

35. Giuliani, A. & Poves, A. Neutrinoless Double-Beta Decay. *Advances in High Energy Physics* **2012**, 1–38 (2012).

36. Pauli W. Neutrino hypothesis in beta-decay. *Letter to participants of Tubingen conference on radioactivity* (1930).

37. Fermi E. Versuch einer Theorie der Betastrahlen. *Zeitschrift fur Physik Bd* **88**, 161–177 (1934).

38. Majorana, E. Teoria simmetrica dell'elettrone e del positrone. *Il Nuovo Cimento* **14**, 171–184 (1937).

39. Konopinski, E. J. & Mahmoud, H. M. The Universal Fermi Interaction. *Physical Review* **92**, 1045–1049 (1953).

40. Goldhaber, M., Grodzins, L. & Sunyar, A. W. Helicity of Neutrinos. *Physical Review* **109**, 1015–1017 (1958).

41. Glashow, S. L. Partial-symmetries of weak interactions. *Nuclear Physics* **22**, 579–588 (1961).

42. Fukuda, Y. *et al.* Evidence for Oscillation of Atmospheric Neutrinos. *Phys Rev Lett* **81**, 1562–1567 (1998).

43. D'Andrea, V. *et al.* Neutrinoless Double Beta Decay with Germanium Detectors: 1026 yr and Beyond. *Universe* **7**, 341 (2021).

44. Siegbahn, K. & Hayward, E. Alpha-, Beta-, and Gamma-Ray Spectroscopy. *Phys Today* **18**, 76–76 (1965).

45. Fiorini, E., Pullia, A., Bertolini, G., Cappellani, F. & Restelli, G. A search for lepton non-conservation in double beta decay with a germanium detector. *Physics Letters B* **25**, 602–603 (1967).

46. Fiorini, E., Pullia, A., Bertolini, G., Cappellani, F. & Restelli, G. An underground experiment on neutrinoless double beta-decay. *Lettere al Nuovo Cimento* **3**, 149–152 (1970).

47. Fiorini, E., Pullia, A., Bertolini, G., Cappellani, F. & Restelli, G. Neutrinoless double-beta decay of76Ge. *Il Nuovo Cimento A* **13**, 747–763 (1973).

48. Forster, A., Kwon, H., Markey, J. K., Boehm, F. & Henrikson, H. E. Low background study of the neutrinoless double beta decay of 76-GE and upper limit for neutrino mass. *Physics Letters B* **138**, 301–303 (1984).

49. Simpson, J. J., Jagam, P., Campbell, J. L., Malm, H. L. & Robertson, B. C. New Limit for Neutrinoless Double β Decay of ^{76}Ge. *Phys Rev Lett* **53**, 141–143 (1984).

50. Fisher, P. *et al.* A search for double beta decay in 76Ge. *Physics Letters B* **218**, 257–262 (1989).

51. Reusser, D. *et al.* Final report on the search for neutrinoless double-β decay of ^{76}Ge from the Gotthard underground experiment. *Physical Review D* **45**, 2548–2551 (1992).

52. Avignone, F. T. *et al.* Ultralow background Study of Neutrinoless Double β Decay of ^{76}Ge: New Limit of the Majorana Mass of υ_e. *Phys Rev Lett* **54**, 2309–2312 (1985).

53. Avignone, F. T. *et al.* New Limits on the Neutrino Mass, Lepton Conservation, and No-Neutrino Double Beta Decay of ^{76}Ge. *Phys Rev Lett* **50**, 721–724 (1983).

54. Avignone, F. T. *et al.* Search for the double- β decay of ^{76}Ge. *Phys Rev C* **34**, 666–677 (1986).

55. Caldwell, D. O. *et al.* Limits on neutrinoless $\beta\beta$ decay, including that with majoron emission. *Phys Rev Lett* **59**, 419–422 (1987).

56. Caldwell, D. O. Double beta decay-present and future. *Journal of Physics G: Nuclear and Particle Physics* **17**, S137–S144 (1991).

57. Klapdor-Kleingrothaus, H. V. *et al.* Latest results from the HEIDELBERG-MOSCOW double beta decay experiment. *The Eur. Phys. Jour. A* **12**, 147–154 (2001).

58. Aalseth, C. E. *et al.* IGEX ^{76}Ge neutrinoless double-beta decay experiment: Prospects for next generation experiments. *Physical Review D* **65**, 092007 (2002).

59. Balysh, A. *et al.* The Heidelberg-Moscow double beta decay experiment with enriched 76Ge. First results. *Physics Letters B* **283**, 32–36 (1992).

60. Balysh, A. *et al.* Sub-eV limit for the neutrino mass from 76Ge double beta decay by the HEIDELBERG-MOSCOW experiment. *Physics Letters B* **356**, 450–455 (1995).

61. Günther, M. *et al.* Heidelberg-Moscow ββ experiment with Ge: Full setup with five detectors. *Physical Review D* **55**, 54–67 (1997).

62. Bakalyarov, A. M., Balysh, A. Ya., Belyaev, S. T., Lebedev, V. I. & Zhukov, S. v. Results of the experiment on investigation of Germanium-76 double beta decay. Experimental data of Heidelberg-Moscow collaboration November 1995 - August 2001. (2003).

63. Aalseth, C. E. *et al.* IGEX ^{76}Ge neutrinoless double-beta decay experiment: Prospects for next generation experiments. *Physical Review D* **65**, 092007 (2002).

64. Ackermann, K.-H. *et al.* The Gerda experiment for the search of 0νββ decay in 76Ge. *The Eur. Phys. Jour. C* **73**, 2330 (2013).

65. Agostini, M. *et al.* Upgrade for Phase II of the Gerda experiment. *The Eur. Phys. Jour. C* **78**, 388 (2018).

66. Results from phase I of the GERDA experiment. *AIP Conference Proceedings* **1686**, 020026 (2015).

67. Agostini, M. *et al.* Final Results of GERDA on the Search for Neutrinoless Double-β Decay. *Phys Rev Lett* **125**, 252502 (2020).

68. Knapp, M. *et al.* The Gerda muon veto Cherenkov detector. *Nucl Instrum Methods Phys Res A* **610**, 280–282 (2009).

69. Abgrall, N. *et al.* The MAJORANA DEMONSTRATOR Neutrinoless Double-Beta Decay Experiment. *Adv. in High Energy Physics* **2014**, 1–18 (2014).

70. Guinn, I. *et al.* Low Background Signal Readout Electronics for the Majorana Demonstrator. *J Phys. Conf. Ser.* **606**, 012009 (2015).

71. Agostini, M. *et al.* Final Results of GERDA on the Search for Neutrinoless Double-β Decay. *Phys. Rev. Lett.* **125**, 252502 (2020).

72. Agostini, M. *et al.* Characterization of inverted coaxial ^{76}Ge detectors in GERDA for future double-β decay experiments. *The European Physical Journal C* **81**, 505 (2021).

73. Alduino, C. *et al.* The projected background for the CUORE experiment. *The Eur. Phys. Jour. C* **77**, 543 (2017).

74. Adams, D. Q. *et al.* Search for Majorana neutrinos exploiting millikelvin cryogenics with CUORE. *Nature* **604**, 53–58 (2022).

75. Armatol, A. *et al.* Novel technique for the study of pileup events in cryogenic bolometers. *Phys Rev C* **104**, 015501 (2021).

76. Newton, I. Philosophiae naturalis principia mathematica. *Jussu Societatis Regiae ac Typis Josephi Streater. Prostat apud plures bibliopolas*, (1687).

77. Adams, J. C. *Manuscripts of John Couch Adams on the perturbations of Uranus*. (1846).

78. Johann Gottfried Galle and the First Observation of Planet Neptune. *http://scihi.org/johann-gottfried-galle-neptune/*.

79. Lundmark. Meddelande frn Lunds astronomiska Observatorium. (1930).

80. Rubin, V. C., Thonnard, N. & Ford, W. K., Jr. Rotational properties of 21 SC galaxies with a large range of luminosities and radii, from NGC 4605 /R = 4kpc/ to UGC 2885 /R = 122 kpc/. *Astrophys J* **238**, 471 (1980).

81. Chae, K.-H. *et al.* Constraints on Cosmological Parameters from the Analysis of the Cosmic Lens All Sky Survey Radio-Selected Gravitational Lens Statistics. *Phys Rev Lett* **89**, 151301 (2002).

82. Gaillard, M. K., Grannis, P. D. & Sciulli, F. J. The standard model of particle physics. *Rev Mod Phys* **71**, S96–S111 (1999).

83. Roszkowski, L., Sessolo, E. M. & Trojanowski, S. WIMP dark matter candidates and searches—current status and future prospects. *Reports on Progress in Physics* **81**, 066201 (2018).

84. Klasen, M., Pohl, M. & Sigl, G. Indirect and direct search for dark matter. *Prog Part Nucl Phys* **85**, 1–32 (2015).

85. Goodman, J. *et al.* Constraints on dark matter from colliders. *Physical Review D* **82**, 116010 (2010).

86. Bertone, G., Hooper, D. & Silk, J. Particle dark matter: evidence, candidates, and constraints. *Phys Rep* **405**, 279–390 (2005).

87. López-Corredoira, M. *et al. Gaia* -DR2 extended kinematical maps. *Astron Astrophys* **634**, A66 (2020).

88. Barnabé-Heider, M. *et al.* Response of superheated droplet detectors of the PICASSO dark matter search experiment. *Nucl Instrum Methods Phys Res A* **555**, 184–204 (2005).

89. Mayet, F. *et al.* A review of the discovery reaches of directional Dark Matter detection. *Phys Rep* **627**, 1–49 (2016).

90. Vahsen, S. E., O'Hare, C. A. J. & Loomba, D. Directional Recoil Detection. *Ann. Rev. of Nucl. and Part. Science* **71**, 189–224 (2021).

91. Aprile, E. *et al.* Excess electronic recoil events in XENON1T. *Physical Review D* **102**, 072004 (2020).

92. Aprile, E. *et al.* Search for New Physics in Electronic Recoil Data from XENONnT. *Phys Rev Lett* **129**, 161805 (2022).

93. Aprile, E. *et al.* Material radiopurity control in the XENONnT experiment. *The Eur. Phys. Jour. C* **82**, 599 (2022).

94. Murra, M., Schulte, D., Huhmann, C. & Weinheimer, C. Design, construction and commissioning of a high-flow radon removal system for XENONnT, *Eur. Phys. J. C*, pre-print, (2022).

95. Pato, M. *et al.* Complementarity of dark matter direct detection targets. *Physical Review D* **83**, 083505 (2011).

96. Newstead, J. L., Jacques, T. D., Krauss, L. M., Dent, J. B. & Ferrer, F. Scientific reach of multiton-scale dark matter direct detection experiments. *Physical Review D* **88**, 076011 (2013).

97. Angloher, G. *et al.* The COSINUS project: perspectives of a NaI scintillating calorimeter for dark matter search. *The Eur. Phys. Jour. C* **76**, 441 (2016).

98. Angloher, G. *et al.* Simulation-based design study for the passive shielding of the COSINUS dark matter experiment. *The Eur. Phys. Jour. C* **82**, 248 (2022).

99. Rau, W. *et al.* Results and status of the CRESST experiment. *J Phys Conf Ser* **39**, 75–81 (2006).

100. CRESST collaboration *et al.* First results on low-mass dark matter from the CRESST-III experiment. *Jour. of Phys.: Conf. Series* **134**, 012076 (2020).

101. Antonello, M. *et al.* The SABRE project and the SABRE Proof-of-Principle. *The European Physical Journal C* **79**, 363 (2019).

102. Morciano, P. *et al.* Fruit Flies Provide New Insights in Low-Radiation Background Biology at the INFN Underground Gran Sasso National Laboratory (LNGS). *Radiat Res* **190**, 217 (2018).

103. Esposito, G. *et al.* Underground Radiobiology: A Perspective at Gran Sasso National Laboratory. *Front Public Health* **8**, (2020).

104. Hall, G. Radiobiology for the Radiologist. *Joanna Cotler Books*, (2006).

105. Esposito, G. *et al.* Underground Radiobiology: A Perspective at Gran Sasso National Laboratory. *Front Public Health* **8**, (2020).

106. Satta, L. *et al.* Low environmental radiation background impairs biological defence of the yeast Saccharomyces cerevisiae to chemical radiomimetic agents. *Mutation Research Letters* **347**, 129–133 (1995).

107. Satta, L. *et al.* Influence of a low background radiation environment on biochemical and biological responses in V79 cells. *Radiat Environ Biophys* **41**, 217–224 (2002).

108. Hall, J. The SNOLAB underground laboratory. in *Journal of Physics: Conference Series* vol. 1468 (Institute of Physics Publishing, 2020).

109. Zarubin, M., Gangapshev, A., Gavriljuk, Y., Kazalov, V. & Kravchenko, E. First transcriptome profiling of D. melanogaster after development in a deep underground low radiation background laboratory. *PLoS One* **16**, e0255066 (2021).

110. Gavriljuk, Ju. M. *et al.* Working characteristics of the New Low background Laboratory (DULB-4900). *Nucl Instrum Methods Phys Res A* **729**, 576–580 (2013).

111. Morciano, P. *et al.* Fruit Flies Provide New Insights in Low-Radiation Background Biology at the INFN Underground Gran Sasso National Laboratory (LNGS). *Radiat Res* **190**, 217 (2018).

112. Jillings, C. The SNOLAB Science Program. *J Phys Conf Ser* **718**, 062028 (2016).

113. Thome, C. *et al.* The REPAIR Project: Examining the Biological Impacts of Sub-Background Radiation Exposure within SNOLAB, a Deep Underground Laboratory. *Radiat Res* **188**, 470–474 (2017).

114. Porrazzo, A. *et al.* Reduced Environmental Dose Rates Are Responsible for the Increased Susceptibility to Radiation-Induced DNA Damage in Larval Neuroblasts of Drosophila Grown inside the LNGS Underground Laboratory. *Int J Mol Sci* **23**, 5472 (2022).

115. Munita, C. S., Glascock, M. D. & Hazenfratz, R. Neutron Activation Analysis: An Overview. *Bentham Books* 179–227 (2019).

116. Sakoda, A. *et al.* First model of the effect of grain size on radon emanation. *Applied Radiation and Isotopes* **68**, 1169–1172 (2010).

117. Aggarwal, S. K. Alpha-particle spectrometry for the determination of alpha emitting isotopes in nuclear, environmental and biological samples: past, present and future. *Anal. Meth.* **8**, 5353–5371 (2016).

118. Spekt et al. Fundamentals of gamma spectrometry. *ISSN 1865-8725* (2018).

119. Hall, M. R. *et al.* γ-ray spectroscopy of astrophysically important states in ^{39}Ca. *Phys Rev C* **101**, 015804 (2020).

120. Nolan, P. J. *et al.* Gamma-ray spectroscopy experiments for levels in ^{39} K below 8.4 MeV excitation. *Journal of Physics G: Nuclear Physics* **7**, 189–218 (1981).

121. Kryemadhi, A. & Chrestay, K. Gamma ray spectroscopy with a silicon photomultiplier and a LYSO crystal. *Am J Phys* **83**, 378–381 (2015).

122. Becker, J. S. *Inorganic Mass Spectrometry*. (Wiley, 2007). doi:10.1002/9780470517222.

123. Boulyga, S. F. *et al.* Determination of 236U/238U isotope ratio in contaminated environmental samples using different ICP-MS instruments. *J Anal At Spectrom* **17**, 958–964 (2002).

124. Akbar Montaser. Inductively Coupled Plasma Mass Spectrometry, *Wiley-VCH*. (1998).

125. GÖÇMENGİL, G. *et al.* Accurate whole-rock geochemistry analysis by combined ICP-OES and LA-ICP-MS instruments. *Bulletin Of The Mineral Research and Exploration* 1–13 (2021) doi:10.19111/bulletinofmre.947703.

126. Date, A. R. & Gray, A. L. Determination of trace elements in geological samples by inductively coupled plasma source mass spectrometry. *Spectrochim Acta Part B At Spectrosc* **40**, 115–122 (1985).

127. Prohaska, T., Latkoczy, C., Schultheis, G., Teschler-Nicola, M. & Stingeder, G. Investigation of Sr isotope ratios in prehistoric human bones and teeth using laser ablation ICP-MS and ICP-MS after Rb/Sr separation. *J Anal At Spectrom* **17**, 887–891 (2002).

128. Becker, J. S. Mass spectrometry of long-lived radionuclides. *Spectrochim Acta Part B At Spectrosc* **58**, 1757–1784 (2003).

129. Becker, J. S. & Dietze, H.-J. Precise isotope ratio measurements for uranium, thorium and plutonium by quadrupole-based inductively coupled plasma mass spectrometry. *Fresenius J Anal Chem* **364**, 482–488 (1999).

130. Feldmann, I., Tittes, W., Jakubowski, N., Stuewer, D. & Giessmann, U. Performance characteristics of inductively coupled plasma mass spectrometry with high mass resolution. *J Anal At Spectrom* **9**, 1007 (1994).

131. Newman, A. Product Review: Elements of ICPMS. *Anal Chem* **68**, 46A-51A (1996).

132. Becker, S. & Dietze, H.-J. Mehrfach geladene ionen kondensierter aromatischer ringsysteme in Funken-Massenspektren. *Int J Mass Spectrom Ion Process* **54**, 337–339 (1983).

133. Bonner, R. F., March, R. E. & Durup, J. Effect of charge exchange reactions on the motion of ions in three-dimensional quadrupole electric fields. *Intern. Jour. of Mass Spec. and Ion Physics* **22**, 17–34 (1976).

134. Douglas, D. J. & French, J. B. Collisional focusing effects in radio frequency quadrupoles. *J Am Soc Mass Spectrom* **3**, 398–408 (1992).

135. Douglas, D. J. Applications of collision dynamics in quadrupole mass spectrometry. *J Am Soc Mass Spectrom* **9**, 101–113 (1998).

136. Becker, J. S. & Dietze, H.-J. Inorganic mass spectrometric methods for trace, ultratrace, isotope, and surface analysis. *Int J Mass Spectrom* **197**, 1–35 (2000).

137. Tanner, S. D. & Baranov, V. I. A dynamic reaction cell for inductively coupled plasma mass spectrometry (ICP-DRC-MS). II. Reduction of interferences produced within the cell. *J Am Soc Mass Spectrom* **10**, 1083–1094 (1999).

138. Boulyga, S. F. & Becker, J. S. Comment on "Isotope ratio measurement by hexapole ICP-MS: mass bias effect, precision and accuracy" by Q. Xie and R. Kerrich, J. Anal. At. Spectrom., 2002, 17, 69. *J. Anal. At. Spectrom.* **17**, 965–966 (2002).

139. Tanner, S. D., Baranov, V. I. & Bandura, D. R. Reaction cells and collision cells for ICP-MS: a tutorial review. *Spectrochim Acta Part B At Spectrosc* **57**, 1361–1452 (2002).

140. Bandura, D. R., Baranov, V. I. & Tanner, S. D. Effect of collisional damping and reactions in a dynamic reaction cell on the precision of isotope ratio measurements. *J Anal At Spectrom* **15**, 921–928 (2000).

141. Wilschefski, S. & Baxter, M. Inductively Coupled Plasma Mass Spectrometry: Introduction to Analytical Aspects. *Clinical Biochemist Reviews* **40**, 115–133 (2019).

142. Yadav, L. D. S. Mass Spectroscopy (MS). in *Organic Spectroscopy* 250–294 (Springer Netherlands, 2005). doi:10.1007/978-1-4020-2575-4_8.

143. Dawson, P. H., Hedman, J. W. & Whetten, N. R. A Simple Mass Spectrometer. *Rev. of Scien. Inst.* **40**, 1444–1450 (1969).

144. Akbar Montaser. Inductively Coupled Plasma Mass Spectrometry, *Wiley-VCH*. (1991).

145. H. E. Duckworth, R. C. B. V. S. V. *Mass Spectroscopy*. (1990).

146. Wieser, M. E. & Schwieters, J. B. The development of multiple collector mass spectrometry for isotope ratio measurements. *Int J Mass Spectrom* **242**, 97–115 (2005).

147. Taylor. *Inductively Coupled Plasma-Mass Spectrometry*. (Elsevier, 2001). doi:10.1016/B978-0-12-683865-7.X5000-5.

148. Nisi, S., di Vacri, A., di Vacri, M. L., Stramenga, A. & Laubenstein, M. Comparison of inductively coupled mass spectrometry and ultra-low-level gamma-ray spectroscopy for ultra-low background material selection. *App. Rad. and Isot.* **67**, 828–832 (2009).

149. Paige, E. G. S. The drift mobility of electrons and holes in germanium at low temperatures. *Journal of Physics and Chemistry of Solids* **16**, 207–219 (1960).

150. Winkler, C. Ueber das Germanium, dessen Nachweis und Bestimmung. *Fresenius' Zeitschrift für analytische Chemie* **26**, 359–364 (1887).

151. Höll, R., Kling, M. & Schroll, E. Metallogenesis of germanium—A review. *Ore Geol Rev* **30**, 145–180 (2007).

152. Rosenberg, E. Germanium: environmental occurrence, importance and speciation. *Rev Environ Sci Biotechnol* **8**, 29–57 (2009).

153. Ruiz, A. G., Sola, P. C. & Palmerola, N. M. Germanium: Current and Novel Recovery Processes. *Adv. Mat. and Device Appl. with Germ.* (InTech, 2018). doi:10.5772/intechopen.77997.

154. Moskalyk, R. R. Review of germanium processing worldwide. *Miner Eng* **17**, 393–402 (2004).

155. Abrosimov, N. *et al.* Technology development of high purity germanium crystals for radiation detectors. *J Cryst Growth* **532**, 125396 (2020).

156. Yang, G. *et al.* Zone Refinement of Germanium Crystals. *J Phys Conf Ser* **606**, 012014 (2015).

157. Wang, G., Mei, H., Mei, D., Guan, Y. & Yang, G. High purity germanium crystal growth at the University of South Dakota. *J Phys Conf Ser* **606**, 012012 (2015).

158. Abgrall, N. *et al.* The processing of enriched germanium for the Majorana Demonstrator and R&D for a next generation double-beta decay experiment. *Nucl Instrum Methods Phys Res A* **877**, 314–322 (2018).

159. J. H. Wernick et al. Techniques and Results of Zone Refining Some Metals. *J. Electrochem. Soc* **106**, (1959).

160. WL Li, Y. L. The review of high purity metal produced by zone refining. *Min. Metall* (2010).

161. Wang, G. *et al.* Development of large size high-purity germanium crystal growth. *J Cryst Growth* **352**, 27–30 (2012).

162. Pfann, W. G. Techniques of Zone Melting and Crystal Growing. *Solid State Physics* **4**, 423–521 (1957).

163. Xu, S. *et al.* Preparation of high purity indium by chemical purification: Focus on removal of Cd, Pb, Sn and removal mechanism. *Hydrometallurgy* **200**, 105551 (2021).

164. Yang, G. *et al.* Zone Refinement of Germanium Crystals. *J Phys Conf Ser* **606**, 012014 (2015).

165. Foot, R. Mirror dark matter and the new DAMA/LIBRA results: A simple explanation for a beautiful experiment. *Physical Review D* **78**, 043529 (2008).

166. Agnes, P. *et al.* First results from the DarkSide-50 dark matter experiment at Laboratori Nazionali del Gran Sasso. *Physics Letters B* **743**, 456–466 (2015).

167. Antonello, M. *et al.* The SABRE project and the SABRE Proof-of-Principle. *The European Physical Journal C* **79**, 363 (2019).

168. Shutt, T. *et al.* The XENON dark matter experiment. *Nucl Phys B Proc Suppl* **138**, 156–159 (2005).

169. Roth, S. *et al.* Direct dark matter search with CRESST and EURECA. *Prog Part Nucl Phys* **64**, 457–459 (2010).

170. Gütlein, A. *et al.* The COSINUS project: Development of new NaI-based cryogenic detectors for direct dark matter search. *Nucl Instrum Methods Phys Res A* **845**, 359–362 (2017).

171. Kaether, F., Hampel, W., Heusser, G., Kiko, J. & Kirsten, T. Reanalysis of the Gallex solar neutrino flux and source experiments. *Physics Letters B* **685**, 47–54 (2010).

172. Bellini, G. *et al.* Final results of Borexino Phase-I on low-energy solar neutrino spectroscopy. *Physical Review D* **89**, 112007 (2014).

173. Caminata, A. *et al.* Results from the Cuore Experiment †. *Universe* **5**, 10 (2019).

174. Ackermann, K.-H. *et al.* The Gerda experiment for the search of 0νββ decay in 76Ge. *The European Physical Journal C* **73**, 2330 (2013).

175. Balogh, L. *et al.* Copper electroplating for background suppression in the NEWS-G experiment. *Nucl Instrum Methods Phys Res A* **988**, 164844 (2021).

176. Cebrián, S. *et al.* Cosmogenic activation in germanium and copper for rare event searches. *Astroparticle Physics* **33**, 316–329 (2010).

177. Atintoh, A., Kpobie, W., Bonfoh, N., Fendler, M. & Lipinski, P. Characterization of the mechanical behavior of a Printed Circuit Board (PCB). in *2021 22nd Inter. Conf. on Thermal, Mechanical and Multi-Physics Sim. and Exp. in Microel. and Micr. (EuroSimE)* 1–5 (IEEE, 2021).

178. Geselbracht, M. J., Ellis, A. B., Penn, R. L., Lisensky, G. C. & Stone, D. S. Mechanical Properties of Metals: Experiments with Steel, Copper, Tin, Zinc, and Soap Bubbles. *J Chem Educ* **71**, 254 (1994).

179. Laubenstein, M. & Lawson, I. Low Background Radiation Detection Techniques and Mitigation of Radioactive Backgrounds. *Front Phys* **8**, (2020).

Acknowledgements

Having reached the end of my studies, I must thank those who have allowed me to get to this point in various ways.

I thank my tutors Stefano Nisi and Marcello Crucianelli, for all the fundamental and precious support given to me during these years of work, their advice and teachings will be fundamental for the continuation of my work; the coordinator and past-coordinator of the doctorate Massimilano Aschi and Antonio Mecozzi for their unconditional support over the years and their assistance in the bureaucratic part of the doctorate.

The entire staff of the Chemistry and Chemical Plant Service of the Gran Sasso National Laboratories, the service manager Marco Balata, Pina, Patrizia, Marco, Andrea, Francesca; for allowing me to work with them over the years.

All my doctoral work at LNGS was possible thanks to the will of Dr Matthias Laubenstein, thank you very much for giving me the opportunity to work in the LEGEND collaboration before and in the Chemistry Service after; you gave me a dream!!

LEGEND spokesman prof. Stefan Schoenert, you gave me the opportunity to work for the first year as a member of your group, everything I learned is and will be invaluable throughout the rest of my career. The whole LEGEND collaboration, working in a totally different context than where I came from made me grow as a chemist, thanks for everything!!

The young colleagues and friends of LNGS with whom I have shared a large part of my work, between comparisons and precious suggestions all my work has always gone towards improvement ... thank you very much Lorenzo, Andrei, Riccardo, Valerio, Roberto, Danilo and all the others…

I thank the Research Division, the Management and the various Services of the LNGS who have given me support and collaboration over the years, always responding to my requests and almost always finding an excellent solution.

The University of L'Aquila and the entire Department of Physical and Chemical Sciences, thank you for leaving me free to pursue my interests. I will never stop thanking fellow PhD students, post-docs, researchers with whom I have dealt with countless times over the years.

All this work has allowed me to fully enter the Italian chemical society and in particular in the mass spectrometry division, fantastic friends and colleagues with whom to share our common passion for chemistry and spectrometry; thank you so much for all our science and fun gatherings!!

I thank my family, my relatives and my friends who have supported me throughout my university years reaching this PhD result!!

I thank the whole ski and scout environment, I grew up with you and I still continue to grow; every race and every field is always an excellent opportunity for comparison and collaboration!!

I thank the Fiori di Nardo association, you made me discover the Holy Land for the first time, from there my interaction with the Israeli chemical society also began; sharing and exchanging ideas will help me in my continuation as a man and scientist.

I thank all the people who have been close to me during this PhD journey, always giving me useful advice and fundamental support.

“Look wide, beyond your immediate surroundings and limits,

and you see things in their right proportion.

Look above the level of things around you and see a higher aim

and possibility to your work.”

Baden Powell